Available online at www.sciencedirect.com
SCIENCE DIRECT®
ELSEVIER
Ocean Engineering 33 (2006) 1161–1213
OCEAN ENGINEERING
www.elsevier.com/locate/oceaneng

On-line identification and convergence analysis of excitation-force and drag-force models for moored floating structures

Mario Alberto Jordán *

Dto. de Ingeniería Eléctrica, Universidad Nacional del Sur, Av. Alem 1253, 8000 Bahía Blanca, Argentina

Received 8 December 2004; accepted 17 May 2005
Available online 1 December 2005

Abstract

This work presents an approach to identify hydrodynamic models for incident, diffraction and viscous forces acting on a moored floating structure. An important aspect treated here is the analysis of the unknown initial condition of the hydrodynamic state for the potential-radiation force. There is established its influence on the parameter convergence and the long-term effects. Afterwards the persistency of excitation of the regressor is analyzed in the case of both poor and rich excitation conditions. Theoretical results show that asymptotic convergence of the estimates takes place under arbitrary conditions of the wave excitation. A case study consisting in the identification of a moored semisubmersible is carried out to exemplify the application of the approach.

Keywords: On-line identification; Persistency of excitation; Moored floating structure; Drag-force model; Excitation-force model; Incidental-force model

1. Introduction

In this paper an approach to the on-line identification of models for excitation and viscous-drag forces of moored floating structures is addressed. The class of floating systems included here encompasses semisubmersibles, buoys, barges, pontoons, crane ships, oil tanks, among the most common used in ocean engineering.

* Tel.: +54 291 459 5100/3310; fax: +54 291 459 5154.
E-mail address: mjordan@criba.edu.ar.

0029-8018/$ - see front matter © 2005 Published by Elsevier Ltd.
doi:10.1016/j.oceaneng.2005.05.016

The importance of attaining accurate models relies mainly on control requirements like dynamic positioning of the floating system around fixed positions and also on the needs of stability analysis like research of forced behaviors with nonlinear oscillations.

From the point of view of the hydrodynamics, an ocean–engineering system interacts with the liquid environment, in particular with waves. This interaction is subject to incidental, diffraction, radiation-induced forces and viscous-drag forces (Faltisen, 1990). A common mathematical approach for the analysis of the forces is the linear Theory of Airy, which relies on the assumption that excitation waves have small steepness (Sorensen, 1993). Incoming-wave forces are however divided into linear components of first-order and nonlinear components of second-orders accounting for the low-frequency drift caused on the body (Clauss et al., 1982). In particular, potential radiation forces are induced from the motion of the floating body with a memory effect which vanishes asymptotically in time (Cummins, 1962; Jiang, 1991). A common property of all hydrodynamic loads is that they cannot be directly measured. Additionally, the initial hydrodynamic state for determining the time evolution of potential radiation forces is unknown.

The requirements of interpreting complex nonlinear dynamic behaviors and also modifying them by means of control systems are habitually satisfied with the use of models (Fossen, 1994). Physical models can provide a more accurate and appropriate basis for analysis, design and simulation tasks than mathematical models since they accurately capture all phenomenological effects and the true model structure. The determination of physical models for ocean–engineering systems has been usually accomplished through experimental tests carried out on structures in reduced scales with the help of onerous test facilities (Chakrabarti, 1994). On the other side, many of the ocean–engineering systems nowadays are equipped with a basic instrumentation that enables the registration of numerous state variables and signals of their behaviors. They provide a common mean for achieving control, fault diagnosis and supervision purposes. Other direct possibility is to construct the model via parameter estimation using these measured data on-line.

The employment of on-line methods of the Estimation Theory may have numerous advantages with respect to the empirical way via test facilities. First on-line estimated models can be identified using the true excitation of the dynamics, it is, the same one that perturbs the functional operation of the floating structure. Second, they can be obtained at a relatively lower effort, time and costs (Ljung, 1987). Finally, many parametric modifications of the system and environment succeed periodically like variation of the system mass, initial tension of mooring lines, changes of the depth during tide and flood, variable wave spectrum, amplitude frequency and incoming angle among others. These changes can be actualized in model if some proper techniques of adaptation of parameters are applied on-line. With a continuously updated model, self-tuning of controller coefficients and adaptive controllers for periodic changes of the system coefficients are also possible (Ioannou and Sun, 1995).

As a moored floating structure is composed by many subsystems actuating interactively, namely the mooring-line system, the potential-radiation hydrodynamics, the Froude–Kriloff excitation and the viscous drag, then a complete estimation may be performed by integrating the estimations of each subsystem as schematically shown in Fig. 1. An approach to identify coefficients of mooring lines in dynamic operation with

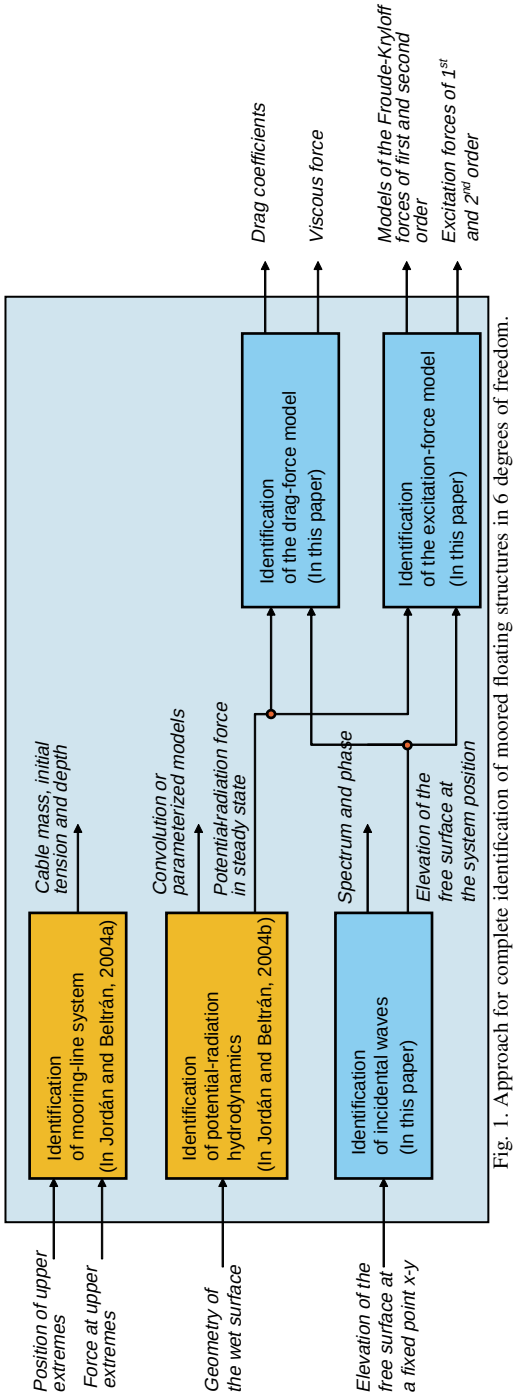

Fig. 1. Approach for complete identification of moored floating structures in 6 degrees of freedom.

measures of the forces and position at their upper extremes is presented in Jordán and Beltrán-Aguedo (2004a). The estimation of potential-radiation models is analyzed in Jordán and Beltrán-Aguedo (2004b). In the present work, we complete the identification of the whole system. The additional subsystems are identified with the measure of mechanical states, the wave elevation at a certain coordinates and the reconstruction in time of the potential-radiation force with initial hydrodynamic state equal to zero.

Due to the numerous parameters involved in the estimation, the question emerges whether it is possible to estimate them under arbitrary conditions of the excitation. The worst case, but also one of the most important in the application, is described by monochromatic waves. As this kind of excitation usually possesses a poor richness of information for identification, a rigorous study of the so-called persistency of excitation (PE property) is needed. This analysis will categorically determine whether the estimation algorithms employed in the parameter identification are able to converge asymptotically or not under such poor but real conditions of excitation. Other important aspect in the analysis is the effect of the initial hydrodynamic state of the potential-radiation force in the parameter convergence, which is unknown. All these features will be considered in the analysis and design of estimation algorithms.

The paper is organized as follows. In the first part, phenomenological laws for the system dynamics are presented. Afterwards, a regression for the estimation is established with the analysis of the initial state for the radiation hydrodynamics using concepts of the Hyperstability Theory. Later, the design and convergence proof of suitable estimation algorithms in continuous time are presented in form of theorems for the cases of mono- and multichromatic waves, respectively. Finally, simulation results for the identification of models for excitation and viscous-drag forces are exemplified for a general case of a moored semisubmersible.

2. Dynamics of a moored floating structure

2.1. General considerations

The dynamics of a moored floating system is considered in 6 degrees of freedom. Accordingly, three pure translations are possible along the longitudinal, transversal and vertical directions of the structure, and three pure rotations are possible about each one of these directions (see Fig. 2). The six motions are termed surge, sway, heave, roll, pitch and yaw, respectively. For these motions an earthbound reference coordinating system parallel to the main directions with the origin at the point O on the water line is selected. In this way the position and the orientation of the structure are given by a generalized position vector $\mathbf{y}=[x,y,z,\varphi,\theta,\psi]^{\mathrm{T}}$ containing the six pure motions in the same order as introduced above. Accordingly, $\dot{\mathbf{y}}$ and $\ddot{\mathbf{y}}$ are the generalized velocity and acceleration vectors, respectively. In addition, it will be useful to indicate the rotation separately as $\boldsymbol{\alpha}=(\varphi,\theta,\psi)^{\mathrm{T}}$.

The structure is anchored to the sea bed by means of a system of symmetrically spread mooring lines. The sea depth from the bed to the still water level is denoted by d. Regular monochromatic waves are assumed to income from a direction with angle β with respect to

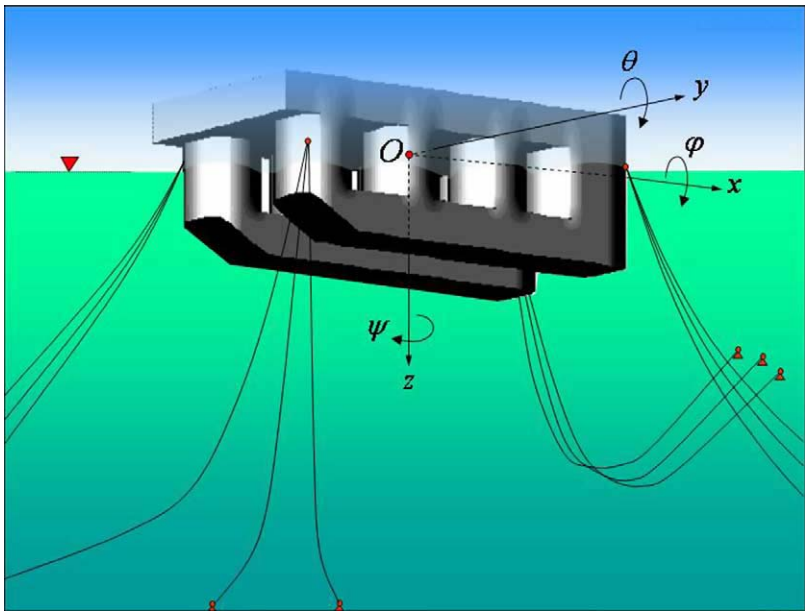

Fig. 2. Conventions for coordinate frame in a semisubmersible.

the x-axis, and to be of amplitude a, frequency ω and length λ. An usually incorporated ballast system enables an horizontal balance of the structure with respect to the free surface in still water. This will be taken as a reference initial position in this work.

The mathematical description is mainly based on the moving equations of rigid body, the interaction fluid–structure and the interaction structure–mooring system.

2.1.1. Assumptions

The modelling will rest on the following assumptions:

(a) A small wave steepness ($2a/\lambda < 1/50$) is considered such that Linear Potential Theory (Airy's Theory) can be applied.
(b) The sea depth for operation of a floating system is supposed intermediate and constant.
(c) The structure is perfectly balanced by the ballast system at hydrostatic equilibrium, i.e. $\varphi_0 = \theta_0 = \psi_0 = 0$ degree in still water.
(d) The mass of the structure is symmetrically distributed with respect to the plane x–z.
(e) The initial tensions of the mooring lines at hydrostatic equilibrium are equal.
(f) The mass of the set of mooring lines is negligible in comparison to the structure mass.
(g) No sloshing phenomenon in ballast system is taken into account.

The modelling of a moored ocean–engineering system can be developed in three stages. First, the equations for the dynamics of the structure conceives as a rigid body are obtained in generalized coordinates. Hereafter, the interaction between fluid and structure together

with the description of the rest of the acting forces is derived. Finally, the characterization of the complete dynamics in space state form is presented.

2.1.2. Notations

Matrices are denoted by capital letters while vectors are in bold. Variables and constants are denoted in italic. Transforms, functional norms and sets are written in calligraphic. The zero vector is referred to as $\mathbf{0}$, the null matrix as 0 and the identity matrix as I, all of them with the corresponding dimension given in the context. The symbol '$\times$' is referred to the outer product and the symbol '$:=$' will denote a definition of a variable into an equation. Norms of vectors and induced norms of matrices are represented by '$\|\cdot\|$'. Finally, estimates are characterized with the symbol '$\wedge$' over the variable name.

2.2. Rigid body dynamics

The dynamics equations for the moored structure are determined by setting up the change of the linear and angular momentums. Starting point for the linear momentum $\mathbf{H}_L$ is the position vector $\mathbf{r}_G$ of the gravity center rotated in $\boldsymbol{\alpha}$ from initial position $(0, 0, \bar{z}_G, 0, 0, 0)^{\mathrm{T}}$. Analogously, the angular momentum $\mathbf{H}_A$ is established with respect to the system coordinates O. Hence

$$\dot{\mathbf{H}}_{L_O} = m\ddot{\mathbf{r}}_G \tag{1}$$

$$\dot{\mathbf{H}}_{A_O} = \dot{\mathbf{H}}_{A_G} + m\mathbf{r}_G \times \ddot{\mathbf{r}}_G, \tag{2}$$

with m the system mass matrix, $\mathbf{H}_L$, $\mathbf{H}_{A_O}$ and $\mathbf{H}_{A_G}$ are the linear and angular momentums with respect to O and G. In generalized coordinates, it results in

$$M(\mathbf{y})\ddot{\mathbf{y}} + \mathbf{K}(\mathbf{y}, \dot{\mathbf{y}}) = \begin{bmatrix} \sum_i F_i \\ \sum_i F_i \times r_{A_i O} \end{bmatrix}, \tag{3}$$

where F_i are the external forces, $F_i \times r_{A_i O}$ the moment caused by F_i with respect to O in a rotation $\boldsymbol{\alpha}$ about it, $r_{A_i O}$ is the distance between the force application point A_i and O.

The matrix $M(\mathbf{y})$ is the generalized inertia matrix

$$M(\mathbf{y}) = \begin{bmatrix} m & 0 & 0 & 0 & m_1 & m_2 \\ 0 & m & 0 & -m_1 & 0 & -m_3 \\ 0 & 0 & m & -m_2 & m_3 & 0 \\ 0 & -m_1 & -m_2 & I_{x_G x_G} + m_4 & m_5 & -I_{x_G z_G} + m_6 \\ m_1 & 0 & m_3 & m_5 & I_{y_G y_G} + m_7 & m_8 \\ m_2 & -m_3 & 0 & -I_{x_G z_G} + m_6 & m_8 & I_{z_G z_G} + m_9 \end{bmatrix}, \tag{4}$$

with $I_{x_G x_G}$, $I_{y_G y_G}$, $I_{z_G z_G}$ and $I_{x_G z_G}$ the inertia moments with respect to the x_G-, y_G-, z_G-axes which have origin at G and are parallel to the x-, y-, z-axes, and m_1 till m_9 functions of $\boldsymbol{\alpha}$

having the form

$$\begin{aligned}
m_1(\boldsymbol{\alpha}) &= m\bar{z}_G \cos\varphi \cos\theta,\\
m_2(\boldsymbol{\alpha}) &= m\bar{z}_G(\sin\varphi\cos\psi - \cos\varphi\sin\theta\sin\psi),\\
m_3(\boldsymbol{\alpha}) &= -m\bar{z}_G(\sin\varphi\sin\psi + \cos\varphi\sin\theta\cos\psi),\\
m_4(\boldsymbol{\alpha}) &= -m\bar{z}_G^2[(\sin\varphi\cos\psi - \cos\varphi\sin\theta\sin\psi)^2 + \cos^2\varphi\cos^2\theta],\\
m_5(\boldsymbol{\alpha}) &= m\bar{z}_G^2[\sin^2\varphi\sin\psi\cos\psi - \cos^2\varphi\sin^2\theta\sin\psi\cos\psi\\
&\quad + \sin\varphi\cos\varphi\sin\theta(2\cos^2\psi - 1)],\\
m_6(\boldsymbol{\alpha}) &= -m\bar{z}_G^2[\sin\varphi\cos\varphi\cos\theta\sin\psi + \cos^2\varphi\sin\theta\cos\theta\cos\psi],\\
m_7(\boldsymbol{\alpha}) &= m\bar{z}_G^2[(\sin\varphi\sin\psi + \cos\varphi\sin\theta\cos\psi)^2 + \cos^2\varphi\cos^2\theta],\\
m_8(\boldsymbol{\alpha}) &= m\bar{z}_G^2[\sin\varphi\cos\varphi\cos\theta\cos\psi - \cos^2\varphi\sin\theta\cos\theta\sin\psi],\\
m_9(\boldsymbol{\alpha}) &= m\bar{z}_G^2[\cos^2\varphi\sin^2\theta + \sin^2\varphi].
\end{aligned} \tag{5}$$

Finally, $\mathbf{K}(\mathbf{y}, \dot{\mathbf{y}})$ contains the generalized centrifugal and Coriolis forces

$$K(\mathbf{y}, \dot{\mathbf{y}}) = \begin{bmatrix} m_3\dot{\theta}^2 + m_3\dot{\psi}^2 \\ m_2\dot{\varphi}^2 + m_2\dot{\psi}^2 \\ -m_1\dot{\varphi}^2 - m_1\dot{\theta}^2 \\ m_8\dot{\theta}^2 - m_8\dot{\psi}^2 \\ -m_6\dot{\varphi}^2 + m_6\dot{\psi}^2 \\ m_5\dot{\varphi}^2 - m_5\dot{\theta}^2 \end{bmatrix} + \begin{bmatrix} -m_2\dot{\varphi}\dot{\theta} + m_1\dot{\varphi}\dot{\psi} \\ -m_3\dot{\varphi}\dot{\theta} + m_1\dot{\theta}\dot{\psi} \\ -m_3\dot{\varphi}\dot{\psi} - m_2\dot{\theta}\dot{\psi} \\ m_6\dot{\varphi}\dot{\theta} - m_5\dot{\varphi}\dot{\psi} + m_4\dot{\theta}\dot{\psi} \\ -m_8\dot{\varphi}\dot{\theta} + m_{10}\dot{\varphi}\dot{\psi} + m_5\dot{\theta}\dot{\psi} \\ m_{11}\dot{\varphi}\dot{\theta} + m_8\dot{\varphi}\dot{\psi} - m_6\dot{\theta}\dot{\psi} \end{bmatrix}, \tag{6}$$

with m_{10} and m_{11} also functions of $\boldsymbol{\alpha}$ with the expression

$$\begin{aligned}
m_{10}(\boldsymbol{\alpha}) &= -m\bar{z}_G^2[(\sin\varphi\sin\psi + \cos\varphi\sin\theta\cos\psi)2 - \cos^2\varphi\cos^2\theta]\\
m_{11}(\boldsymbol{\alpha}) &= m\bar{z}_G^2[\cos^2\varphi\sin^2\theta(2\cos^2\psi - 1) + 4\sin\varphi\cos\varphi\sin\theta\sin\psi\cos\psi\\
&\quad + \sin^2\varphi(1 - 2\cos^2\psi)].
\end{aligned} \tag{7}$$

2.3. Generalized forces

In the following, the generalized forces indicated on the right side of (3) are derived. They comprise the forces caused by mooring lines, structure weight, hydrostatic buoyancy, hydrodynamic loads like incidental, diffraction, potential-radiation and viscous drag forces.

2.3.1. Generalized mooring forces

The mooring forces act on the structure at the attached points with coordinates $(x_{1_i}, y_{1_i}, z_{1_i})$ depending on $\mathbf{y}$. The force and the moment respect to O produced by each mooring line i are obtained in the following way.

First, if the chain length L satisfies

$$L \geq (z_{0_i} - z_{1_i}) \sqrt{\frac{2H_i}{m_c g (z_{0_i} - z_{1_i})}},$$

then the generalized force at the attached point i is

$$\mathbf{F}_{m_i}(\mathbf{y}) = \begin{bmatrix} H_i \cos(\alpha_i) \\ H_i \sin(\alpha_i) \\ m_c g (z_{0_i} - z_{1_i}) \sqrt{\dfrac{2H_i}{m_c g (z_{0_i} - z_{1_i})}} \\ H_i \sin(\alpha_i) z_{c_i} + m_c g (z_{0_i} - Z_1) \sqrt{\dfrac{2H_i}{m_c g (z_{0_i} - z_{1_i})}} y_{c_i} \\ H_i \cos(\alpha_i) z_{c_i} + m_c g (z_{0_i} - z_{1_i}) \sqrt{\dfrac{2H_i}{m_c g (z_{0_i} - z_{1_i})}} x_{c_i} \\ H_i \cos(\alpha_i) y_{c_i} + H_i \sin(\alpha_i) x_{c_i} \end{bmatrix}, \tag{8}$$

with H_i being the horizontal component of the peak tension and obtained implicitly from

$$H_i \to \frac{H_i}{m_c g} \left[\cosh\left(\frac{m_c g}{H_i} l \right) - 1 \right] - (z_{0_i} - z_{1_i}) = 0, \tag{9}$$

$$l = \sqrt{(x_{0_i} - x_{1_i})^2 + (y_{0_i} - y_{1_i})^2}, \tag{10}$$

where m_c is the mass of the line per length units, α_i the line angles in a top view with respect to direction x, $(x_{0_i}, y_{0_i}, z_{0_i})$ the coordinates of the attached points at sea bed and

$$\begin{bmatrix} x_{c_i} \\ y_{c_i} \\ z_{c_i} \end{bmatrix} = T_0(\boldsymbol{\alpha}) \begin{bmatrix} \bar{x}_{c_i} \\ \bar{y}_{c_i} \\ \bar{z}_{c_i} \end{bmatrix}, \tag{11}$$

with $(\bar{x}_{c_i}, \bar{y}_{c_i}, \bar{z}_{c_i})$ the coordinates of the attached points at hydrostatic equilibrium, $(x_{c_i}, y_{c_i}, z_{c_i})$ the coordinates of them after a rotation $\boldsymbol{\alpha}$ and T_0 a transformation matrix given by

$$T_0(\boldsymbol{\alpha}) = T_z(\psi) T_y(\theta) T_x(\varphi), \tag{12}$$

$$T_z(\psi) = \begin{bmatrix} \cos(\psi) & -\sin(\psi) & 0 \\ \sin(\psi) & \cos(\psi) & 0 \\ 0 & 0 & 1 \end{bmatrix}, \tag{13}$$

$$T_y(\theta) = \begin{bmatrix} \cos(\theta) & 0 & \sin(\theta) \\ 0 & 1 & 0 \\ -\sin(\theta) & 0 & \cos(\theta) \end{bmatrix}, \tag{14}$$

$$T_x(\varphi) = \begin{bmatrix} 1 & 0 & 0 \\ 0 & \cos(\varphi) & -\sin(\varphi) \\ 0 & \sin(\varphi) & \cos(\varphi) \end{bmatrix}. \tag{15}$$

If, on the other hand, the chain length L satisfies

$$(z_{0_i} - z_{1_i})\sqrt{\frac{2H_i}{m_c g(z_{0_i} - z_{1_i})}} > L \geq \sqrt{l^2 + (z_{0_i} - z_{1_i})^2},$$

then

$$\mathbf{F}_{m_i}(\mathbf{y}) = \begin{bmatrix} H_i \cos(\alpha_i) \\ H_i \sin(\alpha_i) \\ m_c g L \\ H_i \sin(\alpha_i) z_{c_i} + m_c g L y_{c_i} \\ H_i \cos(\alpha_i) z_{c_i} + m_c g L x_{c_i} \\ H_i \cos(\alpha_i) y_{c_i} + H_i \sin(\alpha_i) x_{c_i} \end{bmatrix}, \tag{16}$$

with

$$H_i \to \frac{H_i L}{m_c g L} \sinh \frac{m_c g L}{H_i} - l = 0, \tag{17}$$

where l is given in (10). Here, it was assumed that any line will not tear up if

$$L \geq \sqrt{(x_{0_i} - x_{1_i} - x)^2 + (y_{0_i} - y_{1_i} - y)^2 + (z_{0_i} - z_{1_i} - z)^2}. \tag{18}$$

The resultant of all catenary generalized forces $\mathbf{F}_{m_i}$ is termed $\mathbf{F}_m$.

2.3.2. Generalized structure weight

The action of the gravity on the structure is obtained by the structure weight force

$$\mathbf{F}_g(\mathbf{y}) = \begin{bmatrix} 0 \\ 0 \\ mg \\ mgy_G \\ mgx_G \\ 0 \end{bmatrix}, \tag{19}$$

where

$$\begin{bmatrix} x_G \\ y_G \end{bmatrix} = \begin{bmatrix} \bar{z}_G(\sin\varphi\sin\psi + \cos\varphi\sin\theta\cos\psi) \\ \bar{z}_G(-\sin\varphi\cos\psi + \cos\varphi\sin\theta\sin\psi) \end{bmatrix} \tag{20}$$

results from a rotation in $\boldsymbol{\alpha}$ of the vector $(0, 0, \bar{z}_G)^{\mathrm{T}}$.

2.3.3. Generalized hydrostatic buoyancy

Assuming calm water and the structure rotated in $\boldsymbol{\alpha}$, the hydrostatic force acts on the metacentric point of coordinates referred to as $(x_m,y_m,z_m)^{\mathrm{T}}$ whose position at hydrostatic equilibrium is $(0, 0, \bar{z}_m)^{\mathrm{T}}$ with $\bar{z}_m$ the metacentric height. The hydrostatic generalized force is

$$\mathbf{F}_b(\mathbf{y}) = \begin{bmatrix} 0 \\ 0 \\ -mg - \rho g A_w z \\ -(mg + \rho g A_w z) y_m \\ -(mg + \rho g A_w z) x_m \\ 0 \end{bmatrix}, \tag{21}$$

with ρ the density of water, A_w the structure water plane area and

$$\begin{bmatrix} x_m \\ y_m \\ z_m \end{bmatrix} = \begin{bmatrix} \bar{z}_m(\sin\varphi\sin\psi + \cos\varphi\sin\theta\cos\psi) \\ \bar{z}_m(-\sin\varphi\cos\psi + \cos\varphi\sin\theta\sin\psi) \\ \bar{z}_m(\cos\varphi\cos\theta) \end{bmatrix}, \tag{22}$$

the metacentric position after rotation.

2.3.4. Generalized potential-radiation force

The induced structure motion due to wave load causes radiation. This radiation is captured according to the linear Theory of Airy as potential-radiation loads influencing the inertia and kinematics of the dynamics. They are associated with radiated waves in an ideal fluid and can be stated in the time domain by means of state-space-model approaches (Jiang, 1991; Schelin et al., 1993; Jordán and Beltrán-Aguedo, 2003) or a convolution approach (Cummins, 1962; Olgivie, 1964). This is

$$\mathbf{F}_h(\mathbf{y}, \mathbf{s}_0) = -M_a\ddot{\mathbf{y}} + \mathbf{s}_0, \tag{23}$$

with M_a the so-called added mass matrix or hydrodynamic mass matrix for a frequency equal to infinite

$$M_a = \mathrm{diag}(a_{x_\infty}, a_{y_\infty}, a_{z_\infty}, a_{\varphi_\infty}, a_{\theta_\infty}, a_{\psi_\infty}), \tag{24}$$

and the vector $\mathbf{s}_0$ accomplishing

$$\mathbf{s}_0(t) = -\int_{-\infty}^{t} K(t-\tau)\dot{\mathbf{y}}(\tau)\mathrm{d}\tau, \tag{25}$$

where $K(\tau)$ is a functional matrix of the independent variable τ containing all the memory of the radiated fluid load response. It depends only on the geometry of the wet part of the submersed body. It is noticing that the evolution in time of $\mathbf{F}_h$ depends on the past history of the velocity of the point O, weighted by $K(\tau)$ on $\tau \in [-\infty, \infty]$. It is suitable to decompose $\mathbf{s}_0$ in a measurable and a nonmeasurable part as

$$\mathbf{s}_0(t) = \mathbf{s}_1(t) + \mathbf{s}_2(t), \tag{26}$$

with

$$\mathbf{s}_1(t) = -\int_{0}^{t} K(t-\tau)\dot{\mathbf{y}}(\tau)\mathrm{d}\tau = -\int_{0}^{t} K(\tau)\dot{\mathbf{y}}(t-\tau)\mathrm{d}\tau \tag{27}$$

$$\mathbf{s}_2(t) = -\int_{-\infty}^{0} K(t-\tau)\dot{\mathbf{y}}(\tau)\mathrm{d}\tau. \tag{28}$$

If $\dot{\mathbf{y}}(t)$ is registered up to $t \geq 0$ and the past evolution is considered zero, then $\mathbf{s}_2(t) \equiv 0$.

2.3.5. Generalized hydrodynamic viscous-drag force

Hydrodynamic viscous-drag forces acting on the moving hull are calculated from empirical relationships. The generalized force is considered as

$$\mathbf{F}_v(\dot{\mathbf{y}}) = -\frac{1}{2}\rho\left(C_{D_x}A_x|\dot{x}|\dot{x}, C_{D_y}A_y|\dot{y}|\dot{y}, C_{D_z}A_z|\dot{z}|\dot{z}, C_{D_\varphi}A_\varphi|\dot{\varphi}|\dot{\varphi}, C_{D_\theta}A_\theta|\dot{\theta}|\dot{\theta}, C_{D_\psi}A_\theta|\dot{\psi}|\dot{\psi}\right)^{\mathrm{T}}, \tag{29}$$

where C_{D_j} are empirical drag coefficients and A_j are coefficients that depend on the geometry of the wet hull shape.

2.3.6. Generalized excitation forces

Forces acting on the structure due to incoming waves produce incidental and diffraction loads. They are approximated by the sum of a first-order component and a second-order slowly-varying drift component (Clauss et al., 1982). An important class of waves is the directional stationary wave composed of a infinite number of wave harmonics at discrete frequencies. This is of random stationary nature. Other wave type is the periodic multichromatic wave. The evolution in time for this particular wave with components of amplitude a_i, frequency ω_i, incoming direction β, wave length λ_i, initial phase ϕ_i, with

respect to the coordinate system is referred to as the free surface elevation

$$\xi(x, y, t) = \sum_{i=1}^{N} a_i \cos(\sigma_i), \tag{30}$$

$$\sigma_i = \frac{2\pi}{\lambda_i}(x \cos(\beta - \psi) + y \sin(\beta - \psi)) - \omega_i t + \phi_i, \tag{31}$$

with $(\beta - \psi)$ the wave heading of the wave component i. The wave length is calculated as

$$\lambda_i = \frac{2\pi c}{\omega_i},$$

with c the so-called wave celerity for each component.

For N components, the generalized excitation force acting on the coordinate center point O results

$$\begin{aligned}\mathbf{F}_w(\mathbf{y}, t) = \sum_{i=1}^{N} & \mathbf{H}_{1i} a_i \cos(-k_i(x(t) - x_b)\cos(\beta - \psi(t)) - k_i(y(t) - y_b)\sin(\beta \\ & - \psi(t)) + \omega_{i1} t + \phi_i) + \mathbf{H}_{2i} a_i \sin(-k_i(x(t) - x_b)\cos(\beta - \psi(t)) \\ & - k_i(y(t) - y_b)\sin(\beta - \psi(t)) + \omega_i t + \phi_i) + \zeta_i^2 \mathbf{G}_i,\end{aligned} \tag{32}$$

where x_b and y_b are the coordinates of the measurement point of the free surface elevation with respect to O, k_i is the wave number equal to $(2\pi/\lambda_i)$, and

$$\mathbf{H}_{1i}(\omega_i, \beta - \psi) = (H_{1x_i}, H_{1y_i}, H_{1z_i}, H_{1\varphi_i}, H_{1\theta_i}, H_{1\psi_i})^{\mathrm{T}}, \tag{33}$$

$$\mathbf{H}_{2i}(\omega_i, \beta - \psi) = (H_{2x_i}, H_{2y_i}, H_{2z_i}, H_{2\varphi_i}, H_{2\theta_i}, H_{2\psi_i})^{\mathrm{T}}, \tag{34}$$

$$\mathbf{G}_i(\bar{\omega}, \beta - \psi) = (G_{x_i}, G_{y_i}, G_{z_i}, G_{\varphi_i}, G_{\theta_i}, G_{\psi_i})^{\mathrm{T}}, \tag{35}$$

with gains H_{1j_i}, H_{2j_i}, which are pairs of the real and imaginary parts of the frequency transfer function vector corresponding to the first-order component of $\mathbf{F}_w$ at ω_i. They depends also on the hull form and on the wave heading. Additionally, the gains are state-dependent through the yaw angle, which may vary in stationary state even supposing β constant. It is remarking that the formulation is conceived for a estimation of gains with ψ constant, even when the dynamics occurs in 6 degrees of freedom. Thus the gains estimated are valid for oscillations with moderated variations of ψ.

The term $\zeta_i^2 G$ is the frequency-dependent second-order drift force. It depends on ζ_i^2 defined as

$$\zeta_i^2 = \sum_{i=1}^{N} a_i^2, \tag{36}$$

also on the wave heading and on the hull form. For simplification G_{j_i} is evaluated only for the central frequency $\bar{\omega}$ defined as the algebraic mean of all ω_i.

It is remarkable that a monochromatic wave is a special case of the approach above. Also a stationary random wave with different β_i's can be included in the approach. However, this kind of wave is generally considered of minor importance in the application in comparison to directional waves due to its relatively smaller wave energy. Finally, the approach (32) can be extended nearly to stationary directional waves with continuous spectra by approximating these with a spectrum of lines with finite energy spread at regular discrete frequencies. The treatment for these approximations is given in Section 5.

2.4. System dynamics representation

Combining (3) with (8), (16), (19), (21), (23), (29) and (32), the dynamics of the floating structure is described in the earthbound coordinate system by

$$[M(\mathbf{y}) + M_a]\ddot{\mathbf{y}} + \mathbf{K}(\mathbf{y}, \dot{\mathbf{y}}) = \mathbf{F}_m(\mathbf{y}) + \mathbf{F}_g(\mathbf{y}) + \mathbf{F}_b(\mathbf{y}) + \mathbf{F}_v + \mathbf{F}_w(\mathbf{y}, t) + \mathbf{s}_0(t). \quad (37)$$

There is another form in state-space for representing the dynamics. This will be treated in Section 4 for further analysis.

3. Parameter estimation

3.1. Measures

Taken into account (37) and assuming that $\mathbf{y}, \dot{\mathbf{y}}$ and $\ddot{\mathbf{y}}$ are measurable, then $M(\mathbf{y})$ and $\mathbf{K}(\mathbf{y}, \dot{\mathbf{y}})$ can be reconstructed. Moreover, suppose that by identification of the mooring-line coefficients according to Fig. 1, see also Jordán and Beltrán-Aguedo (2003), $\mathbf{F}_m(\mathbf{y})$ can be rebuilt. Similarly, by identifying the weighting matrix function $K(\tau)$ according to the geometry of the wet surface of the body, the component $\mathbf{s}_0(t)$ of the potential-radiation force and the additive matrix M_a can be determined. However, as noticed before, $\mathbf{s}_0$ is only reproduced with null initial hydrodynamic state, i.e. $\mathbf{s}_0(t) \equiv \mathbf{s}_1(t)$ (see (27) and (28)).

So, using this information, one can simulate the resultant of the excitation and viscous-drag forces by means of the first membership in the equation

$$[M(\mathbf{y}) + M_a]\ddot{\mathbf{y}} + \mathbf{K}(\mathbf{y}, \dot{\mathbf{y}}) - \mathbf{F}_m(\mathbf{y}) - \mathbf{F}_g(\mathbf{y}) - \mathbf{F}_b(\mathbf{y}) - \mathbf{s}_1(t) = \mathbf{F}_v + \mathbf{F}_w(\mathbf{y}, t) + \mathbf{s}_2(t). \quad (38)$$

Clearly, using $\mathbf{s}_1(t)$ instead of $\mathbf{s}_0(t)$ will produce an error that influences the estimates as shown in Section 3.2.

3.2. Regression

In the general case, with a directional stationary random wave of N harmonics $\omega_i \in \{\omega_1, \ldots, \omega_N\}$, the sum of the components for viscous-drag and excitation forces in each motion

mode is expressed by the following regression in vector form according to (29) and (32)

$$\begin{bmatrix} \boldsymbol{\Phi}_x^T(t)\boldsymbol{\theta}_x \\ \boldsymbol{\Phi}_y^T(t)\boldsymbol{\theta}_y \\ \boldsymbol{\Phi}_z^T(t)\boldsymbol{\theta}_z \\ \boldsymbol{\Phi}_\varphi^T(t)\boldsymbol{\theta}_\varphi \\ \boldsymbol{\Phi}_\theta^T(t)\boldsymbol{\theta}_\theta \\ \boldsymbol{\Phi}_\psi^T(t)\boldsymbol{\theta}_\psi \end{bmatrix} = \mathbf{F}_v(t) + \mathbf{F}_w(t), \tag{39}$$

with the associated scalar regressor for the mode $q_i \in \{x,y,z,\varphi,\theta,\psi\}$

$$\begin{aligned} \boldsymbol{\Phi}_{q_i}^T(t) = \Big(& -\dot{q}_i(t)|\dot{q}_i(t)|, a_1 \cos(-k_1(x(t)-x_b)\cos(\beta-\psi(t)) - k_1(y(t)-y_b) \\ & \times \sin(\beta-\psi(t)) + \omega_1 t + \phi_1), a_1 \sin(-k_1(x(t)-x_b)\cos(\beta-\psi(t)) \\ & - k1(y(t)-y_b)\sin(\beta-\psi(t)) + \omega_1 t + \phi_1), \ldots, a \cos(-k_N(x(t)-x_b) \\ & \times \cos(\beta-\psi(t)) - k_N(y(t)-y_b)\sin(\beta-\psi(t)) + \omega_N t + \phi_N), \\ & \times a_N \sin(-k_1(y(t)-x_b)\cos(\beta-\psi(t)) - k_N\,(y(t)-y_b) \\ & \times \sin(\beta-\psi(t)) + \omega_N t + \phi_N), \sum_{i=1}^{N} a_i^2 \Big) \end{aligned} \tag{40}$$

and the true parameter vector for the same mode

$$\boldsymbol{\theta}_{q_i} = \left(\frac{C_{D_{q_i}} A_{q_i} \rho}{2}, H_{1q_i}(\omega_1,\beta), H_{2q_i}(\omega_1,\beta), \ldots, H_{1q_i}(\omega,\beta), H_{2q_i}(\omega,\beta), G_{q_i}(\bar{\omega},\beta) \right)^{\mathrm{T}}. \tag{41}$$

As $\mathbf{F}_v(t)$ and $\mathbf{F}_w(t)$ are unknown, e.g. nonmeasurable, it is thus required to capture them indirectly with the help of (38) as a regression

$$\begin{pmatrix} \boldsymbol{\Phi}_x^T(t)\boldsymbol{\theta}_x \\ \boldsymbol{\Phi}_y^T(t)\boldsymbol{\theta}_y \\ \boldsymbol{\Phi}_z^T(t)\boldsymbol{\theta}_z \\ \boldsymbol{\Phi}_\varphi^T(t)\boldsymbol{\theta}_\varphi \\ \boldsymbol{\Phi}_\theta^T(t)\boldsymbol{\theta}_\theta \\ \boldsymbol{\Phi}_\psi^T(t)\boldsymbol{\theta}_\psi \end{pmatrix} = [M(\mathbf{y}) + M_a]\ddot{\mathbf{y}} + \mathbf{K}(\mathbf{y},\dot{\mathbf{y}}) - \mathbf{F}_m(\mathbf{y}) - \mathbf{F}_g(\mathbf{y}) - \mathbf{F}_b(\mathbf{y}) - \mathbf{s}_1(t) - \mathbf{s}_2(t). \tag{42}$$

Clearly, formulations (39) and (42) are equivalent for $\mathbf{s}_2(t) \equiv 0$.

The number of parameters to be estimated is $12(N+1)$. It depends basically on the number of significative components present in the wave line spectrum.

3.3. Estimation algorithms

For the estimation of the $\boldsymbol{\theta}_{q_i}$'s it is suitable from a mathematical point a view to use a minimization procedure in norm 2. Hence for the estimate vector $\hat{\boldsymbol{\theta}} = (\hat{\boldsymbol{\theta}}_x^T, \hat{\boldsymbol{\theta}}_y^T, \hat{\boldsymbol{\theta}}_z^T, \hat{\boldsymbol{\theta}}_\varphi^T, \hat{\boldsymbol{\theta}}_\theta^T, \hat{\boldsymbol{\theta}}_\psi^T)^T$ consider the following scalar cost functional for the energy of the estimation error

$$\min_{\hat{\boldsymbol{\theta}} \in \Re^{12(N+1)}} J(t, \hat{\boldsymbol{\theta}}) = \min_{\hat{\boldsymbol{\theta}} \in \Re^{12(N+1)}} \frac{1}{2t} \int_0^t \varepsilon^T(\tau, \hat{\boldsymbol{\theta}}) \varepsilon(\tau, \hat{\boldsymbol{\theta}}) \mathrm{d}\tau, \tag{43}$$

with the estimation error

$$\varepsilon(\tau, \hat{\boldsymbol{\theta}}) = [M(\mathbf{y}) + M_a]\ddot{\mathbf{y}} + \mathbf{K}(\mathbf{y}, \dot{\mathbf{y}}) - \mathbf{F}_m(\mathbf{y}) - \mathbf{F}_g(\mathbf{y}) - \mathbf{F}_b(\mathbf{y}) - \mathbf{s}_1(t) - \begin{pmatrix} \boldsymbol{\Phi}_x^T(t)\hat{\boldsymbol{\theta}}_x(t) \\ \boldsymbol{\Phi}_y^T(t)\hat{\boldsymbol{\theta}}_y(t) \\ \boldsymbol{\Phi}_z^T(t)\hat{\boldsymbol{\theta}}_z(t) \\ \boldsymbol{\Phi}_\varphi^T(t)\hat{\boldsymbol{\theta}}_\varphi(t) \\ \boldsymbol{\Phi}_\theta^T(t)\hat{\boldsymbol{\theta}}_\theta(t) \\ \boldsymbol{\Phi}_\psi^T(t)\hat{\boldsymbol{\theta}}_\psi(t) \end{pmatrix}. \tag{44}$$

Now, in order to find minima of J, one employs an adaptation law. If J is uniformly globally convex for $\mathbf{s}_0(0) = 0$ and there exist suitable excitation conditions (see analysis in Section 6), the unique minimum is global and given as the root of J by

$$\frac{\partial J(t, \hat{\boldsymbol{\theta}})}{\partial \hat{\boldsymbol{\theta}}} = \mathbf{0}, \quad \text{implies} \quad \hat{\boldsymbol{\theta}} = \boldsymbol{\theta}. \tag{45}$$

In order to reach the minimum point $\hat{\boldsymbol{\theta}} = \boldsymbol{\theta}$ many algorithms can be applied. We described two significative classes of them.

3.3.1. Gradient-based algorithm

The parameter trajectory is forced to follow the way of steepest descending path over J according to the adaptive law

$$\dot{\hat{\boldsymbol{\theta}}} = -\Gamma \frac{\partial J(t, \hat{\boldsymbol{\theta}})}{\partial \hat{\boldsymbol{\theta}}} = \frac{\Gamma}{t} \int_0^t \Phi^T(\tau) \varepsilon(\tau, \hat{\boldsymbol{\theta}}) \mathrm{d}\tau, \tag{46}$$

with $\hat{\boldsymbol{\theta}}(0) = 0$, $\Gamma = \Gamma^{\mathrm{T}} > 0$ a gain matrix, $\boldsymbol{\Phi}(\tau) = \mathbf{d}iag(\boldsymbol{\Phi}_x^T(\tau), \boldsymbol{\Phi}_y^T(\tau), \boldsymbol{\Phi}_z^T(\tau), \boldsymbol{\Phi}_\varphi^T(\tau), \boldsymbol{\Phi}_\theta^T(\tau), \boldsymbol{\Phi}_\psi^T(\tau))$ and $\boldsymbol{\varepsilon} = \Phi(\boldsymbol{\theta} - \hat{\boldsymbol{\theta}})$. The trajectory will converge to the equilibrium point $\hat{\boldsymbol{\theta}} = \boldsymbol{\theta}$ under necessary and sufficient conditions for $t \to \infty$. Also, the integral may be skipped over, obtaining a new estimation algorithm with different convergence to the same equilibrium point (Ioannou and Sun, 1995).

3.3.2. Least-squares-based algorithm

Other possibility is to force the parameter trajectory from an initial condition in direction to some estimation of the equilibrium point at every moment. This is reached by performing the minimization of the integral of the square errors with respect to the parameter vector at every time t. The parameter trajectory is given as the solution of the following ordinary differential equations in vector and matrix forms

$$\dot{\hat{\boldsymbol{\theta}}}(t) = -P(t)\Phi^T(t)\boldsymbol{\varepsilon}(t), \tag{47}$$

$$\dot{P}(t) = -P(t)\Phi^T(t)\Phi(t)P(t), \tag{48}$$

with $\hat{\boldsymbol{\theta}}(0)$ and $P(0)>0$. The matrix P is referred to as the covariance matrix and stands for the variance of the parameter errors. The trajectory will converge to the equilibrium point $\hat{\boldsymbol{\theta}} = \boldsymbol{\theta}$ under certain necessary and sufficient conditions for $t \to \infty$.

4. Vanishing effect of the initial hydrodynamic state

The inexactitude of (42) lies only in the lack of knowledge about the initial state of the potential-radiation force $\mathbf{s}_2(t)$, which is supposed in the analysis before identically zero for all t. So in using $\mathbf{s}_1$ instead of the true $\mathbf{s}_0$ in the regression (42), a transient difference between (39) and (42) will be generally occur, which is zero only in the particular case that both the environment and the floating structure are at rest at $t_0=0$, i.e. no excitation is present. In the next we will study the influence of this uncertainty in the estimation.

As seen below in this section, the vanishing rate of the transient state depends mainly on the amplitude of $\dot{\mathbf{q}}$. It is noticed that the dissipation of the mechanics and hydrodynamic energy will depend mainly on two forces: the viscous-drag and the linear damping forces. Most notably is the viscous-drag force that dissipates a significant energy with a power proportional to the quadratic value of $\dot{\mathbf{q}}$. Important in accounting for the magnitude of this force is the effective area presented to the motion direction and that $|\dot{\mathbf{q}}| > 1$. On the other side, the linear damping acts more effective in low-frequency movements of the structure.

4.1. State-space approach of the dynamics

The dynamics of the floating structure plays a fundamental role in the estimation. Consider a suitable state-space characterization of the whole dynamics given by

$$\begin{aligned}
\dot{\mathbf{y}} &= \dot{\mathbf{y}},\\
\ddot{\mathbf{y}} &= [M(\mathbf{y}) + M_a]^{-1}(-\mathbf{K}(\mathbf{y},\dot{\mathbf{y}}) + \mathbf{F}_g(\mathbf{y}) + \mathbf{F}_b(\mathbf{y}) + \mathbf{s}_0 + \mathbf{F}_m(\mathbf{y}) + \mathbf{F}_v(\dot{\mathbf{y}})\\
&\quad + \mathbf{F}_w(\mathbf{y},t)),\\
\dot{\mathbf{s}}_0 &= \frac{\mathrm{d}}{\mathrm{d}t}\left(-\int_0^t K(t-\tau)\dot{\mathbf{y}}(\tau)\mathrm{d}\tau\right),
\end{aligned} \tag{49}$$

with the generalized state vector

$$\mathbf{q} = \begin{bmatrix} \mathbf{y} \\ \dot{\mathbf{y}} \\ \mathbf{s}_0 \end{bmatrix}, \tag{50}$$

initial condition (cf. (25)–(28))

$$\mathbf{q}(0) = [\mathbf{y}^T(0), \dot{\mathbf{y}}^T(0), \mathbf{s}_0^T(0)]^{\mathrm{T}} = [\mathbf{y}^T(0), \dot{\mathbf{y}}^T(0), \mathbf{s}_2^T(0)]^{\mathrm{T}}, \tag{51}$$

and with the condition that $[M(\mathbf{y})+M_a]$ be nonsingular.

Consider (42) as an associated output equation to the state-space model

$$\Phi^T(t)\boldsymbol{\theta} = [M(\mathbf{y}) + M_a]\ddot{\mathbf{y}} + \mathbf{K}(\mathbf{y}, \dot{\mathbf{y}}) - \mathbf{F}_m(\mathbf{y}) - \mathbf{F}_g(\mathbf{y}) - \mathbf{F}_b(\mathbf{y}) - \mathbf{s}_0. \tag{52}$$

More compactly, (49) is

$$\begin{cases} \dot{\mathbf{q}} = \mathbf{f}(\mathbf{q}) + M_0(\mathbf{q}) \begin{pmatrix} \mathbf{0} \\ \mathbf{F}_m(\mathbf{q}) + \mathbf{F}_v(\dot{\mathbf{q}}) + \mathbf{F}_w(\mathbf{q}, t) \\ \mathbf{0} \end{pmatrix}, \\ \Phi^T(t)\boldsymbol{\theta} = \mathbf{F}_v(\dot{\mathbf{q}}) + \mathbf{F}_w(\mathbf{q}, t), \end{cases} \tag{53}$$

with the initial condition (51), $M_0(\mathbf{q}) = \mathrm{diag}(0, [M(\mathbf{q}) + M_a]^{-1}, 0)$ and

$$\mathbf{f}(\mathbf{q}) = \begin{bmatrix} sI \\ \mathbf{0} \\ sI \end{bmatrix} \mathbf{q} + M_0(\mathbf{q}) \begin{bmatrix} \mathbf{0} \\ -\mathbf{K}(\mathbf{q}, \dot{\mathbf{q}}) + \mathbf{F}_g(\mathbf{q}) + \mathbf{F}_b(\mathbf{q}) + (\mathbf{0}, \mathbf{0}, I)\mathbf{q} \\ \mathbf{0} \end{bmatrix}. \tag{54}$$

where s is the Laplace variable and I a 6×6 identity matrix. It is also assumed that $\mathbf{f}$ is bounded in the state space.

In order to analyze the system dynamics we first focus our analysis on the mooring and excitation forces. Toward this goal, one assumes mooring lines with catenary forms during the motion and a whole force–deformation characteristic accomplishing

$$f_{\max}\big(\|q\|\big) \geq \|M_0(\mathbf{q})\mathbf{F}_{M_{q_i}}(\mathbf{q})\| \geq f_{\min}\big(\|q\|\big), \tag{55}$$

with $M_0(\mathbf{q}) > 0$ and $f_{\max}$ and $f_{\min}$ being two upper and lower bounding functions of high order in $\|\mathbf{q}\|$, respectively. The nonlinear mooring forces play a fundamental role in the stabilization of the floating structure.

4.2. Perturbed system dynamics

The data used in identification will be obtained partially by numerical simulation of the potential-radiation hydrodynamics and partially by direct measurement of mechanical system variables. The dynamics that reflects the data via simulation is that one with initial hydrodynamics state $\mathbf{s}_0(0) = \mathbf{s}_2(0) = \mathbf{0}$. This dynamics is referred to as perturbed one and the corresponding state referred to as $\mathbf{q}_\delta$. From this dynamics, it is practically to distinguish

Table 1
System dynamics of a moored floating structure in two environments

(a) Dynamic non-linear system at rest	$\begin{cases} \dot{\mathbf{q}}_\delta = f(\mathbf{q}_\delta) + M_0(\mathbf{q}_\delta)\begin{pmatrix} \mathbf{0} \\ \mathbf{F}_m(\mathbf{q}_\delta) + (\mathbf{0},\mathbf{0},I)\delta\mathbf{q} \\ \mathbf{0} \end{pmatrix}, & \text{for } \mathbf{q}_\delta(0) = \mathbf{q}(0), \\ \Phi_\delta^{\mathrm{T}}(t)\boldsymbol{\theta} = (\mathbf{0},\mathbf{0},I)\delta\mathbf{q}, \end{cases}$
(b) Dynamic oscillating time-varying system	$\begin{cases} \dot{\mathbf{q}}_\delta = \mathbf{f}(\mathbf{q}_\delta) + M_0(\mathbf{q}_\delta), \\ \begin{pmatrix} \mathbf{0} \\ \mathbf{F}_m(\mathbf{q}_\delta) + \mathbf{F}_v(\dot{\mathbf{q}}_\delta) + \mathbf{F}_w(\mathbf{q}_\delta, t) + (\mathbf{0},\mathbf{0},I)\delta\mathbf{q} \\ \mathbf{0} \end{pmatrix}, & \text{for } \mathbf{q}_\delta(0) = \mathbf{q}(0), \\ \Phi_\delta^{\mathrm{T}}(t)\boldsymbol{\theta} = \mathbf{F}_v(\dot{\mathbf{q}}_\delta) + \mathbf{F}_w(\mathbf{q}_\delta, t) + (\mathbf{0},\mathbf{0},I)\delta\mathbf{q}. \end{cases}$

two particular situations, namely, the dynamics at rest and that one induced by monochromatic waves.

The perturbed dynamics can be more appropriately stated from (53) by considering the perturbed state $\mathbf{q}_\delta$ and defining an additive perturbation on the right side being

$$\delta\mathbf{q}(t) = \begin{pmatrix} \mathbf{0} \\ \mathbf{0} \\ -\mathbf{s}_2(t) \end{pmatrix}. \tag{56}$$

So one can establish two perturbed systems in space state corresponding to the dynamics mentioned before. These are indicated in Table 1

The initial condition of the states in the perturbed system is the same as in (53), it is $\mathbf{q}_\delta(0) = \mathbf{q}(0)$ (see (51)).

$$\mathbf{q}_\delta(0) = \begin{bmatrix} \mathbf{y}(0) \\ \dot{\mathbf{y}}(0) \\ \mathbf{s}_0(0) \end{bmatrix} = \begin{bmatrix} \mathbf{y}(0) \\ \dot{\mathbf{y}}(0) \\ \mathbf{s}_2(0) \end{bmatrix} = \mathbf{q}(0). \tag{57}$$

The dynamics (a) in Table 1 is described in blocks in Fig. 3. It is composed by the dynamics of the unconstrained floating structure with a nonlinear feedback implemented

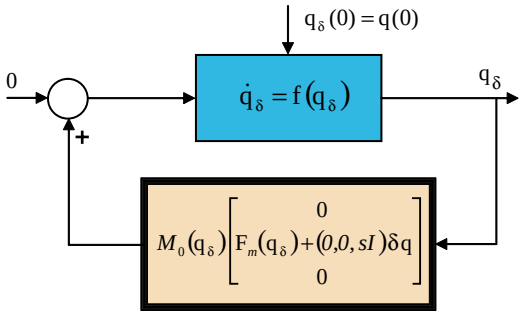

Fig. 3. State-space model of the perturbed moored structure at rest.

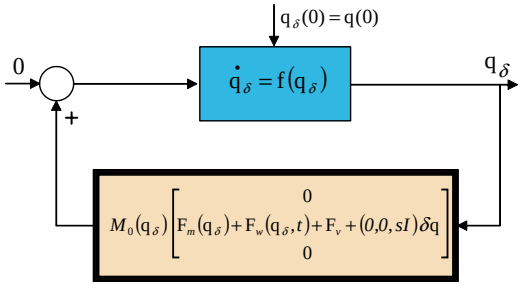

Fig. 4. State-space model of the perturbed moored structure under monochromatic wave excitation.

by the mooring-lines equations. The dynamics (b) in Table 1 is similar as in (a) with an additional nonlinear time-varying feedback reproduced by the state-depending excitation (see Fig. 4). It is noticing that both dynamics represented by control systems have null set points.

It is also observing from (56) and (28) that $\delta\mathbf{q}$ is depending on the past evolution of the system dynamics and hence on the initial condition $\mathbf{q}(0)$. As $\delta\mathbf{q}$ is part of the hydrodynamics, it is indicated in Figs. 3 and 4 as part of the state feedback.

4.3. Initial hydrodynamic state in the system at rest

Consider first the unperturbed dynamic system at rest. From physical principles, it is asymptotically stable inasmuch as the initial condition does lie in the attraction domain of the system. This concerns particularly the critic angles and their derivatives of the pitch and roll modes. The system trajectory moves from the initial condition $\mathbf{q}(0)$ to the equilibrium point $\mathbf{q}^* = [0,0,z_G,0,0,0,0^T,0^T]^T$ asymptotically. The asymptotic stability is mainly ensured due to two classes of damping, namely the nonlinear damping provided by the viscous drag force and the linear hydrodynamic damping characterized by $\mathbf{s}_0$ (49). The first damping decelerates strongly the system by quick motions, while the second one offers resistance to motion during slow motions. However, when the perturbation $\delta\mathbf{q}$ acts on the dynamics, the hydrodynamics state $\mathbf{s}_0(t)$ behaves as $\mathbf{s}_1(t)$ without the past information of $\mathbf{s}_2(t)$. The trajectory of the perturbed state $\mathbf{q}_\delta(t)$ starts from $\mathbf{q}(0)$ but afterwards runs away from the unperturbed system path. Since $\mathbf{s}_0(t)$ tends asymptotically to $\mathbf{s}_1(t)$, both trajectories will touch asymptotically again. Thus the effect of the perturbation $\delta\mathbf{q}$ vanishes in time and the perturbed system is also asymptotically stable having the same equilibrium point $\mathbf{q}^*$ inasmuch as $\mathbf{q}(0)$ remains in the attractive region of the perturbed system. The evolution of the trajectories of the perturbed and unperturbed systems are characterized in Fig. 5 graphically.

4.4. Initial hydrodynamic state in the wave-excited system

On the other side, when the system is excited by a monochromatic wave, the dynamics shows an oscillatory behavior of the same period as that of the wave or a more complex one in bifurcation state with high periods including also the possibility of chaotic orbits

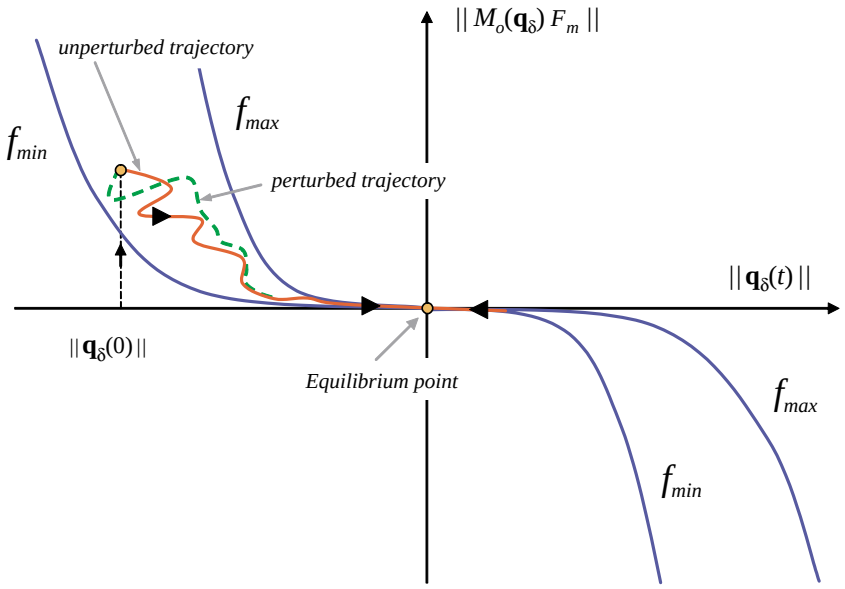

Fig. 5. Trajectories of the perturbed and unperturbed systems at rest.

(Kreuzer et al., 2002). Simultaneously, the drift originated by the nonlinear components of the excitation pushes asymptotically the mean point of the oscillatory motion, which abandons the static equilibrium point to reach a new center displaced in the opposite direction of the incoming wave and with a magnitude proportional to the wave energy.

Consider now the unperturbed system. The trajectory starts from $\mathbf{q}(0)$ and becomes asymptotically a periodic orbit in a forced motion. The perturbed system, on the contrary, behaves similarly under equal excitation, but the influence of $\delta\mathbf{q}$ begins to drive the trajectory on a different path as in the previous case (see Fig. 6). However, as $\delta\mathbf{q}$ vanishes in time, the trajectory returns asymptotically to the same periodic orbit as in the unperturbed case.

The domain of attraction is restricted by certain maximal levels of wave energy that do not cause the structure to turn over. Usually, the capsizing is avoided by implementing a system of many mooring lines that provide sufficiently large stabilizing moments for relatively large angles and displacements.

4.5. Properties of the perturbed state

Consider $K(\tau)$ in (25) again. For floating structures in the Ocean Engineering K is absolutely integrable. Then

$$\int_0^\infty \|K(\tau)\|\, \mathrm{d}\tau < \infty, \tag{58}$$

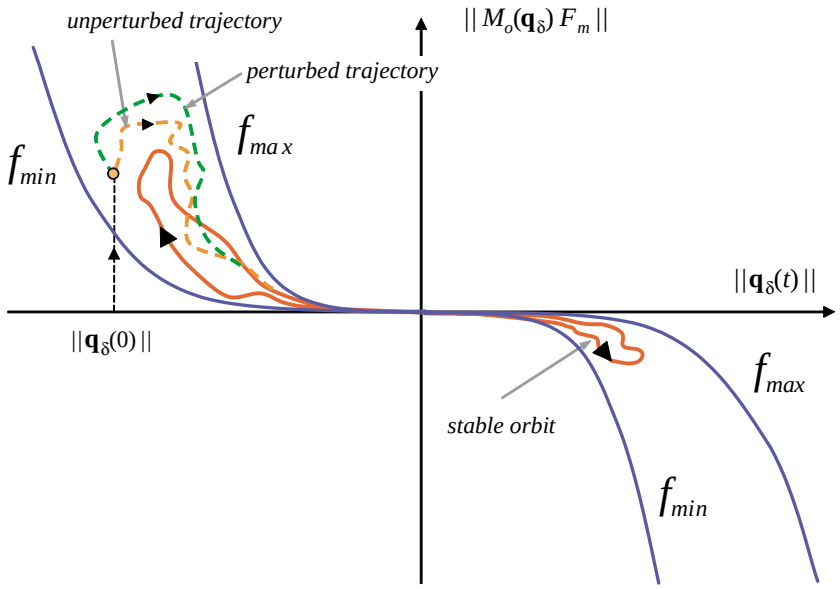

Fig. 6. Trajectories of the perturbed and unperturbed systems under regular excitation.

it means $K(\tau) \in \mathcal{L}_1$. Thus, there exists a Fourier transform function of it with real and imaginary components referred to as $D(\omega)$ and $j\omega M_a(\omega)$, respectively. From the Riemann–Lebesgue Lema (Olgivie, 1964), it follows

$$\lim_{\omega\to\infty} \int_0^\infty K(\tau)\sin(\omega\tau)\mathrm{d}\tau, \tag{59}$$

$$\lim_{\omega\to\infty} \int_0^\infty K(\tau)\cos(\omega\tau)\mathrm{d}\tau = 0, \tag{60}$$

which tells about the continuity of $K(\tau)$. Using this feature, (58) and the Barbălat's Lemma (cf. Ioannou and Sun, 1995), it is valid that $K(\tau)$ is bounded, i.e. $K \in \mathcal{L}_\infty$.

The stability of the hydrodynamics can equivalently be inferred from the property that $D(\omega)$ is continuous. So one gets (Jordán and Beltrán-Aguedo, 2004b)

$$\lim_{\tau\to\infty} K(\tau) = \lim_{\tau\to\infty} \frac{2}{\pi} \int_0^\infty D(\omega)\cos(\omega\tau)\mathrm{d}\omega = 0, \tag{61}$$

which tells about the vanishing effect of the hydrodynamic load in response to a sudden displacement of the structure.

Usually, the frequency transfer function of the hydrodynamics, expressed by $D(\omega) + j\omega M_a(\omega)$, can be fitted accurately by a rational transfer function matrix of appropriate finite

order n (Jordán and Beltrán-Aguedo, 2004b). Thus the decaying of $K(\tau)$ for a linearly increasing τ is also exponential, i.e. there exist matrices A and A_0 of dimension 6×6 so that for $\tau\geq0$ it is valid

$$\|K(\tau)\| \leq \|A_0\, \mathrm{e}^{A\tau}\| = \alpha_0\, \mathrm{e}^{-\alpha\tau}, \tag{62}$$

with α, $\alpha_0>0$.

Consider now the unperturbed system state $\mathbf{q}(t)$ with initial condition $\mathbf{q}(0)$ in (51) and the perturbed system state $\mathbf{q}_\delta(t)$ resulting from (53) with the perturbation $\delta\mathbf{q}(t)$ in (50) and starting from the same initial condition $\mathbf{q}(0)=\mathbf{q}_\delta(0)$. Hence the state error is

$$\mathbf{e}_q(t) = \mathbf{q}(t) - \mathbf{q}_\delta(t). \tag{63}$$

As the control systems described in Figs. 3 and 4 are asymptotically stable, there exists a scalar function $V(t)=(1/2)\mathbf{e}_q^T(t)\mathbf{e}_q(t)$ with $\dot{V}(t)\leq0$. Since $V(t)$ is bounded from below and is not increasing, it has a limit as $t\to\infty$ (see Ioannou and Sun, 1995), it is

$$\lim_{t\to\infty} V(t) = \lim_{t\to\infty} \frac{1}{2} \int_0^t \mathbf{e}_q^T(\tau)\mathbf{e}_q(\tau)\mathrm{d}\tau = V_\infty < \infty.$$

This implies that $\mathbf{e}_\mathrm{q}(t)$ is quadratic integrable (i.e. $\mathbf{e}_q \in \mathcal{L}_2$) and bounded. Because $\mathbf{f}$ is bounded and M_0 is nonsingular, $\dot{\mathbf{e}}_q(t)$ is also bounded on $[0,\infty]$, i.e. $\mathbf{e}_q$, $\dot{\mathbf{e}}_q \in \mathcal{L}_\infty$. Hence, $\mathbf{e}_q(t)$ is also uniformly continuous. In consequence, due to the Barbălat's Lemma (Ioannou and Sun, 1995) one holds

$$\lim_{t\to\infty} \mathbf{e}_q(t) = \mathbf{0}. \tag{64}$$

The property (64) will be invoked below in Section 4.6. It is proved that the difference between the trajectories $\mathbf{q}(t)$ and $\mathbf{q}_\delta(t)$ vanishes in time as indicated graphically in Figs. 5 and 6.

4.6. Properties of the measure error

Consider the perturbed measure vector as indicated in Table 1 for the time-varying system

$$\mathbf{\Phi}_\delta^T(t)\boldsymbol{\theta} = \mathbf{F}_v(\dot{\mathbf{q}}_\delta) + \mathbf{F}_w(\mathbf{q}_\delta, t) + (\mathbf{0},\mathbf{0},I)\delta\mathbf{q} \tag{65}$$

and the corresponding unperturbed vector defined in (39) as

$$\mathbf{\Phi}^T(t)\boldsymbol{\theta} = \mathbf{F}_v(\dot{\mathbf{q}}) + \mathbf{F}_w(\mathbf{q}, t). \tag{66}$$

Taking the difference between both vectors, one gets the measure error

$$\varepsilon_\Phi(t) = (\Phi^T(t) - \Phi_\delta^T(t))\theta = -(0,0,I)\delta\mathbf{q} = -\int_{-\infty}^{0} K(t-\tau)(0,I,0)\mathbf{q}(\tau)\mathrm{d}\tau. \tag{67}$$

According to (62), $K(\tau)$ is exponentially decaying and for every element k_{ij}, there exists

real-valued constants $\alpha_{1_{ij}}$, $\alpha_{2_{ij}}$, $\beta_{1_{ij}}$ and $\beta_{2_{ij}}$, with $\alpha_{1_{ij}} < \alpha_{2_{ij}}$ and $\beta_{1_{ij}} > \beta_{2_{ij}} > 0$, such that

$$\alpha_{1_{ij}} \mathrm{e}^{-\beta_{1_{ij}}\tau} \leq k_{ij}(\tau) \leq \alpha_{2_{ij}} \mathrm{e}^{-\beta_{2_{ij}}\tau}. \tag{68}$$

The first 12 components of $\boldsymbol{\varepsilon}_{\boldsymbol{\Phi}}$ are zero and the last 6 satisfy

$$-\int_{-\infty}^{0} \sum_{j=1}^{6} \alpha_{1_{ij}} \mathrm{e}^{-\beta_{1_{ij}}(t-\tau)} q_i(\tau)\mathrm{d}\tau \geq \varepsilon_{\boldsymbol{\Phi}_{q_i}}(t)$$

$$= -\int_{-\infty}^{0} \sum_{j=1}^{6} k_{ij}(t-\tau) q_i(\tau)\mathrm{d}\tau \geq -\int_{-\infty}^{0} \sum_{j=1}^{6} \alpha_{2_{ij}} \mathrm{e}^{-\beta_{2_{ij}}(t-\tau)} q_i(\tau)\mathrm{d}\tau, \tag{69}$$

with $q_i = \dot{y}_i \in \{\dot{x}, \dot{y}, \dot{z}, \dot{\theta}, \dot{\varphi}, \dot{\psi}\}$ according to the generalized velocity vector $\dot{\mathbf{y}}$. Equivalently

$$-\sum_{j=1}^{6} \frac{\alpha_{1_{ij}}}{\beta_{1_{ij}}} \mathrm{e}^{-\beta_{1_{ij}}t} \sup_{\tau\in[0,t]} (q_i(\tau)) \geq \varepsilon_{\Phi_{q_i}}(t) \geq -\sum_{j=1}^{6} \frac{\alpha_{2_{ij}}}{\beta_{2ij}} \mathrm{e}^{-\beta_{2ij}t} \sup_{\tau\in[0,t]} (q_i(\tau)). \tag{70}$$

Then, it follows from (70) with $\sup_{\tau\in[0,t]}(q_i(\tau)) < \infty$ the property

$$\lim_{t\to\infty} \boldsymbol{\varepsilon}_{\boldsymbol{\Phi}} = 0. \tag{71}$$

The main conclusion that can be derived from the last equation is that the perturbation $\delta\mathbf{q}$ can produce a false measure and its effect is exponentially decreasing in time.

4.7. Properties of the regression matrix

Consider the measure error component $\varepsilon_{\boldsymbol{\Phi}_{q_i}}$. It is valid the relation

$$\int_0^t \varepsilon^2_{\boldsymbol{\Phi}_{q_i}} \,\mathrm{d}\tau = \hat{\boldsymbol{\theta}}^T_{q_i}(t) \int_0^t (\boldsymbol{\Phi}_{q_i}(\tau) - \boldsymbol{\Phi}_{\delta_{q_i}}(\tau))(\boldsymbol{\Phi}_{q_i}(\tau) - \boldsymbol{\Phi}_{\delta_{q_i}}(\tau))^T \,\mathrm{d}\tau\, \hat{\boldsymbol{\theta}}_{q_i}(t). \tag{72}$$

Since $\varepsilon_{\boldsymbol{\Phi}_{q_i}}(t)$ is bounded from below and above, this implies it is quadratic integrable, i.e. $\varepsilon_{\boldsymbol{\Phi}_i} \in \mathcal{L}_2$. In consequence the total energy of the measure error is

$$\lim_{t\to\infty} \int_0^t \varepsilon^2_{\boldsymbol{\Phi}_i}(\tau)\mathrm{d}\tau = c, \tag{73}$$

with c a positive constant vector.

The integral in (72) represents the energy of the error in the measurements that causes the misinformation in the estimation. Moreover, in case of convergence, $\boldsymbol{\Phi}_{q_i}$ must be necessarily persistent exciting (see next theorems) and it is valid

$$\lim_{t\to\infty} \int_0^t \boldsymbol{\Phi}_{q_i} \boldsymbol{\Phi}^T_{q_i} \,\mathrm{d}\tau = \lim_{t\to\infty} \int_0^t \boldsymbol{\Phi}_{\delta_{q_i}} \boldsymbol{\Phi}^T_{\delta_{q_i}} \,\mathrm{d}\tau = \infty, \tag{74}$$

and

$$\lim_{t\to\infty}\frac{\left|\int_0^t(\boldsymbol{\Phi}_{q_i}-\boldsymbol{\Phi}_{\delta_{q_i}})(\boldsymbol{\Phi}_{q_i}-\boldsymbol{\Phi}_{\delta_{q_i}})^T\,\mathrm{d}\tau\right|}{\left|\int_0^t\boldsymbol{\Phi}_{q_i}\boldsymbol{\Phi}_{q_i}^T\,\mathrm{d}\tau\right|}=0. \tag{75}$$

This last statement says, that the misinformation becomes asymptotically insignificant in comparison to the information gained along the time. The parameter trajectory induced by an estimation law based on $\boldsymbol{\Phi}_{\delta_{q_i}}$ will be distorted temporarily in its behavior due to the presence of $\varepsilon_{\boldsymbol{\Phi}_i}$ in comparison with the case of unperturbed measures. At the same time, as the true information begins to cumulate increasingly, the trajectory will be pushed by the adaptive law to move to the true parameter vector.

5. Identification of wave parameters

The measurement of a directional wave elevation is necessary in (40) for the identification of excitation forces on the structure (see Fig. 1). It provides the amplitudes of the fractionated wave components of the wave spectrum and their phases, which is needed for applying the wave parameters in the regressor (40), namely the wave amplitude a_i, the wave number k_i and the wave initial phase ϕ_i of every component in the wave spectrum.

The wave parameters can be estimated from the measurement of the wave elevation at a single-point of the surface. There exist ad hoc surface buoys with instrumentation to achieve this objective. These on-line capture the height of the primary wave above the bottom and perform RF transmission to another reception point (see, for instance, Grosenbaugh, 1996; Tasai et al., 1980; Borgman et al., 2003). In particular, it is assumed here that the sensor buoy is in the neighborhood of the floating structure, which is the receptor of the wave information.

The objective in this section is to develop an estimation method for the wave parameters based on the measurement of the wave elevation at a single point of the ocean. The transmitted wave signal will be synchronized with the sensors of $\mathbf{y}$, $\dot{\mathbf{y}}$ and $\ddot{\mathbf{y}}$ of the floating structure so as to exactly reproduce the excitation forces on the structure according to (38).

Additionally, it is assumed that in the case of a continuous wave spectrum, this can be approximated by a discrete one supported by discrete-time samples of the wave elevation at an appropriate rate. The proper selection of the sample rate is based on following physical arguments. First, it is a physical fact that wave spectra of different geographic regions decrease significantly for frequencies greater than 10 rad/s. Therefore, it implies by Shannon Theorem that the sample rate has not to be larger than $\pi/10=0.314$ s. On the other hand, too small values of the sample rate would lead to irrelevant information of the wave at high frequencies and intolerable time-consuming computations for the spectrum determination. An usual value for the sample time could be 0.1 s, thus the influence of aliasing phenomena on the sampled signal due to the unconsidered portion of the spectrum will be negligible.

We divide our analysis into two cases, both concerning directional waves. The first case describes regular multichromatic waves and the second one focuses realizations of irregular stationary waves. In both cases $\xi(t,x_0,y_0)$ is referred to as the wave elevation at the sensor buoy position, which is digitally registered from $t=t_0$ up to $t=t_0+T$, with t_0 the so-called synchronization time and T the measurement period at the sensor buoy.

5.1. Case 1: Multichromatic waves

Consider a buoy with symmetry in the plane x–y and a periodic wave $\xi(t,x_0,y_0)$ with a wave heading angle equal to β according to (30). Thus it is valid

$$\xi(t,x_0,y_0)=\sum_{i=1}^{N} a_i \sin(k_i(x_0\cos\beta+y_0\sin\beta)+\omega_i t+\phi_i), \tag{76}$$

where ϕ_i is a stochastic phase uniformly distributed between 0 and 2π radians, a_i the amplitude, ω_i the frequencies of the wave components, β the incoming angle, k_i the wave number and (x_0,y_0) the geographic coordinates of the buoy with respect to the floating structure.

The set of wave parameters to be identify is

$$\wp_i=\{a_i,\omega_i,\phi_i,k_i\},\quad i=1,\ldots,N. \tag{77}$$

As the line spectrum has no information of phase, one employs consequently the Fourier Transform of ξ over the measurement interval $[t_0,t_0+T]$, with $T\gg 2\pi/\min\omega_i$ (Bracewell, 1978). Hence, the time-discrete signal

$$\xi'(t_k,x_0,y_0)=w(t_k;t_0,T)\xi(t_k,x_0,y_0), \tag{78}$$

is available from the measured signal with t_k a discrete-time, w a weighting function that satisfies $w(t;t_0,T)=h(t-t_0)-h(t-t_0-T)$ and $h(t)$ a unit step function. Then, for N samples in $[t_0,t_0+T]$ the discrete Fourier transform (DFT) is

$$\Xi_i=\Xi(t_k,x_0,y_0)=\frac{1}{N}\sum_{k=1}^{N} e^{j(2\pi(k-1)(i-1)/N)},\quad \text{for } 1\le i\le N, \tag{79}$$

where $\{\Xi_i\}$ represents a series of complex Fourier coefficients of the DFT, which can be described equivalently in discrete time by

$$\xi_i'=\xi'(t,x_0,y_0)=\sum_{i=1}^{N} a_i\sin(\omega_i t+\phi_i), \tag{80}$$

where the $\{\xi_i'\}$ represents the transmitted signal of the wave elevation to the floating structure.

The estimation of a_i and ϕ_i results from the calculus using the Fourier coefficients $\Xi_i=\alpha_i+j\beta_i$ in the following identity by means of

$$a_i\sin(\omega_i t+\phi_i)=\alpha_i\sin(\omega_i t)+\beta_i\cos(\omega_i t), \tag{81}$$

with

$$a_i \frac{|\alpha_i|}{\cos\left(\tan^{-1}\frac{\beta_i}{\alpha_i}\right)} = \frac{|\beta_i|}{\sin\left(\tan^{-1}\frac{\beta_i}{\alpha_i}\right)}, \tag{82}$$

$$\phi_i = \begin{cases} -\tan^{-1}\dfrac{\beta_i}{\alpha_i} + \dfrac{\pi}{2}, & \text{for } \alpha_i > 0, \\ -\tan^{-1}\dfrac{\beta_i}{\alpha_i} + \dfrac{3\pi}{2}, & \text{for } \alpha_i < 0. \end{cases} \tag{83}$$

The frequencies ω_i and the number N of them must be detected directly from the lines of the series $\{\Xi_i\}$ in (79). The criterion developed in this paper is to define the set of significative lines as

$$S_N = \{a_i \in \mathrm{DFT}[\xi(t_k, x_0, y_0)] | a_i > \varepsilon > 0, \quad i = 1, \ldots, N\}, \tag{84}$$

with ε a threshold for avoiding insignificant amplitudes. Then, for all a_i in the set S_N, one picks up the frequencies ω_i for which (82) and (83) are calculated.

The wave numbers in (77) are univocally calculated a posteriori by means of the implicit relation (Sorensen, 1993)

$$\omega_i^2 = k_i g \tanh(k_i d), \tag{85}$$

where d is the sea depth.

5.1.1. Example

Let $\xi(t_k,x_0,y_0)$ be a multichromatic periodic wave elevation as represented in Fig. 7. The signal is composed by 10 sinus components with stochastically chosen phases and

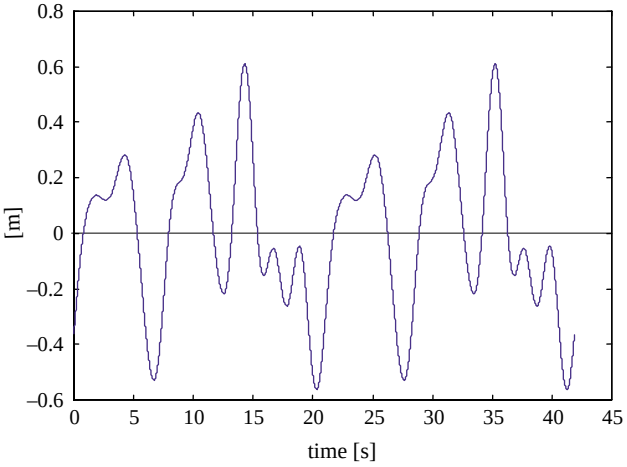

Fig. 7. Directional periodic wave elevation.

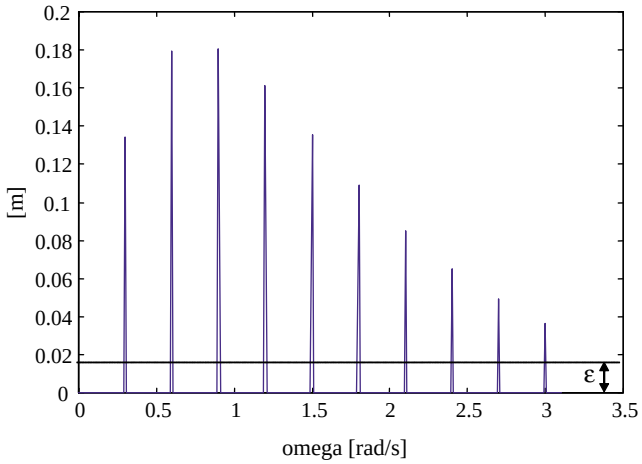

Fig. 8. Amplitudes of the discrete Fourier Transform for a periodic wave elevation.

reproduced with a sample time equal to 0.1 s on [0,T], with T being 30 times the signal period.

After applying the DFT on $\xi(t_k,x_0,y_0)$, (82) and (83) and considering a threshold $\varepsilon = 0.1\ \max_{i=1,\ldots,N}(a_i)$, then 10 harmonics are detected. The unknown amplitudes and phases are identified with insignificant error and shown in Figs. 8 and 9, respectively.

5.2. Case 2: Irregular stationary waves

In the case of irregular stationary waves, the associated spectral density function is continuous in the frequency. The contribution of energy of each wave component of the

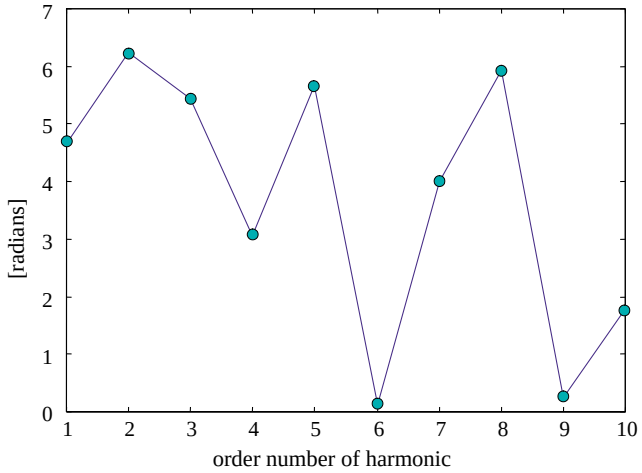

Fig. 9. Estimated phases of the expansion for a periodic wave elevation.

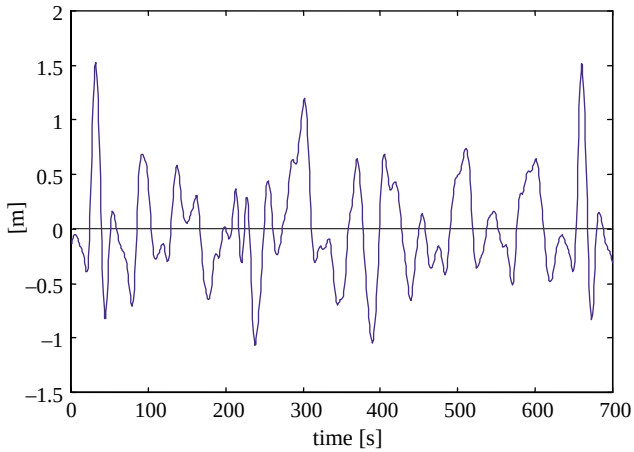

Fig. 10. Directional random wave elevation.

spectrum is infinitesimal. However, by the time sampling of such a wave in a finite period T, a discrete spectrum is generated. For N time samples in T, the spectral lines are placed at discrete frequencies $(i2\pi)/T$, with $i=0,\pm1,\pm2,\ldots,\pm N/2$. In the limit, i.e. for $T\rightarrow\infty$, the discrete spectrum tends asymptotically to the continuous one. For all discrete frequencies the DFT computes the spectral density lines with amplitudes and phases which are equivalent to the pseudo-stochastic signal $\xi(t)=\xi(t+T)$, where $\xi(t)$ on $[0,T]$ is the portion of the sampled irregular wave behavior. Once T and N are fixed, one defines a set of significative lines in the spectrum according to (84).

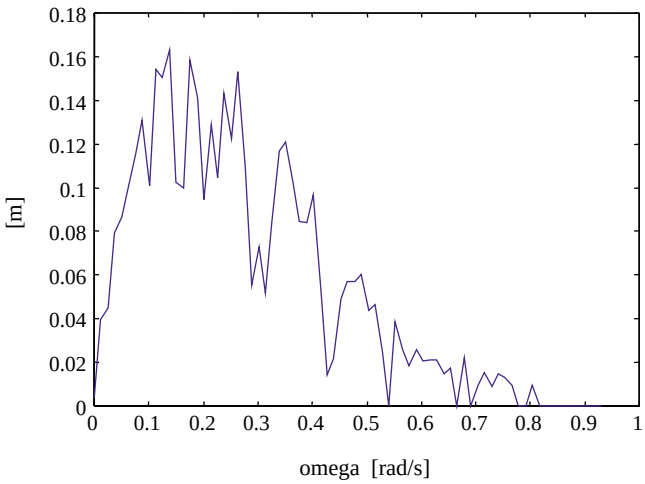

Fig. 11. Amplitudes of the discrete Fourier Transform for a random wave elevation.

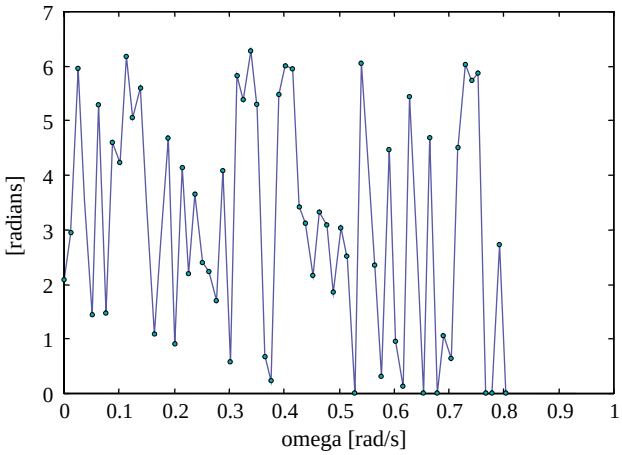

Fig. 12. Estimated phases of the expansion for a random wave elevation.

5.2.1. Example

In Fig. 10 a stationary random wave elevation $\xi(t,x_0,y_0)$ is generated as a stochastic process with the typical wave spectrum of Pierson–Moskowitz. The signal course on a period of $T=700$ s is depicted in Fig. 10.

After applying DFT on $\xi(t_k,x_0,y_0)$, (82) and (83) and considering a threshold $\varepsilon = 0.05\ \max_{i=1,\ldots,N}(a_i)$, then 60 harmonics are detected as meaningful. The identified amplitudes and phases are shown in Figs. 11 and 12, respectively. With these estimates, the wave can be reconstructed with minor errors through the expression (76) for $N=60$.

5.3. Insertion of the wave at the structure sensor point

The information of the buoy sensor has to be transmitted to the estimator, which computes herefrom the wave elevation at the structure site. If the sensor buoy is located on the downstream side with respect to the structure, then the estimator must predict backwards the evolution of the wave elevation at the site of the structure. On the other hand, if the buoy is on the upstream side, the estimator must predict forwards the evolution from the buoy sensor. Only in the particular case when structure and buoy are located in a line, which is perpendicular to the incoming wave direction, the wave elevation is the same at both sites.

If the wave is irregular, the wave elevation is not predictable anywhere. On the contrary, for regular waves a prediction is possible. The problem of prediction the wave elevation at different geographic coordinates is not simple because the wave may propagate with different celerities for each frequency component, i.e.

$$c_i = \frac{\lambda_i \omega_i}{2\pi} = \frac{\omega_i}{k_i}. \tag{86}$$

Hence the predictions does not imply a simple time delay of the elevation $\xi(t)$ because the initial phases ϕ_i change with the location. However, if the measurement of the wave elevation is made at two different points simultaneously with relative coordinates (x_0,y_0)

and corresponding signals

$$\xi_1(t,0,0) = \sum_{i=1}^{N} a_{1i} \sin(\omega_i t + \phi_{1i}), \tag{87}$$

$$\xi_2(t,0,0) = \sum_{i=1}^{N} a_{2i} \sin(\omega_i t + \phi_{2i}), \tag{88}$$

then, according to (76), the initial phases ϕ_{1i} and ϕ_{2i} are related together through

$$\phi_{1i} = k_i(x_0 \cos\beta + y_0 \sin\beta) + \phi_{2i}, \tag{89}$$

and for each harmonic detected by means of the criterium (84) it is valid

$$k_i = \frac{\phi_{1i} - \phi_{2i}}{x_0 \cos\beta + y_0 \sin\beta}.$$

Finally, for the prediction of ξ, it is supposed that the transmitted data are synchronized with the on-board sensors of the structure. Let the structure sensor position O have planar coordinates $(x(t),y(t))$ and the coordinates of the buoy in the fixed frame have coordinates (x_b,y_b). This synchronization is accomplished for the received wave elevation $\xi(t_k,x,y)$, which is transformed by means of the DFT and rearranged for the new coordinates of the sensor position O accordingly to

$$\xi(t,x,y) = \sum_{i=1}^{N} a_i \cos\left(-k_i(x(t)-x_b)\cos(\beta-\psi(t)) - k_i(y(t)-y_b)\sin(\beta-\psi(t)) + \omega_i t + \phi_i + \frac{\pi}{2}\right). \tag{90}$$

This periodic signal is the excitation that accounts for the dynamics of the platform reproduced by the measures $\mathbf{y}$, $\dot{\mathbf{y}}$ and $\ddot{\mathbf{y}}$. Moreover, the coefficients a_i, ω_i, k_i and ϕ_i are needed in the regressor (40) for the intended on-line identification of the excitation-force and drag-force models. For pseudo-periodic signals as described in the Case 2, the prediction for another geographic point is only approximately valid, since the signal is not repeatable after $t > T$.

6. Convergence

The analysis here is concerned with the ability of the estimation algorithms developed in Section 3.3, to converge asymptotically to the true values under important classes of sea excitations. The convergence of the estimation for the incident, diffraction and viscous-drag parameters is first demonstrated for monochromatic excitation and then generalized for directional regular multichromatic waves.

An important part of the convergence proof is based on the concept of persistent of excitation (PE) for finite period of arbitrary length in continuous time, which is necessary condition for analysis of asymptotic and exponential stable adaptive systems. The literature in this area is quite diverse and vast, see for instance, Kreisselmeier and Rietze-

Augst (1990), Narendra and Annaswamy (1987), Ioannou and Sun (1995) and Jordán (2002).

Per definition, a piecewise continuous signal vector $\mathbf{\Phi} : \Re^+ \to \Re^n$ is referred to as PE in $[0,T]$ with a so-called level of excitation $\alpha_0 > 0$ if there exists constants α_1, $T_0 > 0$ and $T_0 \in (0,T]$ such that

$$\alpha_1 I \geq \frac{1}{T_0} \int_t^{t+T_0} \mathbf{\Phi}(\tau)\mathbf{\Phi}^T(\tau)\mathrm{d}\tau \geq \alpha_0 I. \tag{91}$$

The results of this section are presented in form of theorems for a general moored structure described by (37). First it is proved that the regressor vector $\mathbf{\Phi}_{q_i}(t)$ in (40) is PE. Afterwards, the convergence of the algorithms (46), (47) and (48) are proved with the PE condition satisfied.

Theorem 1 (Persistency of excitation—Case: monochromatic wave). *If the floating structure is excited by a monochromatic wave*

$$\xi(t,x,y) = a_0 \cos(-k_0(x-x_b)\cos(\beta-\psi) - k_0(y-y_b)\sin(\beta-\psi) + \omega_0 t + \phi_0), \tag{92}$$

then the regressor $\mathbf{\Phi}_{q_i}(t)$ *in* (40) *with* $N=1$ *is PE.*

Proof. Consider $\mathbf{\Phi}_{q_i} \in \Re^4$ according to (39) for $N=1$ with q_i an arbitrary mode. Using the definition in (91), for $\mathbf{\Phi}_{q_i}$ to be PE it must satisfy

$$\alpha_1 T_0 I \geq \int_t^{t+T_0} \mathbf{\Phi}_{q_i}(\tau)\mathbf{\Phi}_{q_i}^T(\tau)\mathrm{d}\tau \geq \alpha_0 T_0 I, \tag{93}$$

for some level of persistency $\alpha_0 > 0$, some constant $\alpha_1 > 0$ and some period $T_0 > 0$. The former condition is equivalent to

$$\mathrm{span}\{\mathbf{\Phi}_{q_i}(\tau), \quad \text{for } \tau \in [t, t+T_0]\} = \Re^4. \tag{94}$$

which corresponds to generate four vectors $\mathbf{\Phi}_{q_i}(\tau_j)$ for arbitrary and distinct $\tau_j \in [t, t+T_0]$ from the functional basis

$$B(\tau) = \{b_1(\tau), b_2(\tau), b_3(\tau), b_4(\tau)\}, \tag{95}$$

with

$$b_1(\tau) = -\dot{q}_i(\tau)|\dot{q}_i(\tau)|, \tag{96}$$

$$b_2(\tau) = a_1 \cos(-k_1(x(\tau)-x_b)\cos(\beta-\psi(\tau)) - k_1(y(\tau)-y_b)\sin(\beta-\psi(\tau)) + \omega_1\tau + \phi_1), \tag{97}$$

$$b_3(\tau) = a_1 \sin(-k_1(x(\tau)-x_b)\cos(\beta-\psi(\tau)) - k_1(y(\tau)-y_b)\sin(\beta-\psi(\tau)) + \omega_1\tau + \phi_1), \tag{98}$$

$$b_4(\tau) = a_1^2, \tag{99}$$

and to demand for $\{\tau_1,\tau_2,\tau_3,\tau_4\} \in [t,t+T_0]$ that $\sum_{i=1}^{4} \mathbf{\Phi}_{q_i}(\tau_i)\mathbf{\Phi}_{q_i}^T(\tau_i) > 0$, i.e. to be positive definite. More generally, for the last statement to be valid, there must not exist nonzero constants c_j other than zero such that one attains

$$b_1(\tau) = c_1 b_2(\tau), \tag{100}$$

$$b_1(\tau) = c_2 b_3(\tau), \tag{101}$$

$$b_1(\tau) = c_3 b_4(\tau), \tag{102}$$

$$b_2(\tau) = c_4 b_3(\tau), \tag{103}$$

$$b_2(\tau) = c_5 b_4(\tau), \tag{104}$$

$$b_3(\tau) = c_5 b_4(\tau). \tag{105}$$

For (100), the following differential equation is produced with (96) and (97)

$$-\dot{q}_i(\tau)|\dot{q}_i(\tau)| = c_1 a_1 \cos(-k_1(x(\tau)-x_b)\cos(\beta-\psi(\tau)) - k_1(y(\tau)-y_b)\sin(\beta - \psi(\tau)) + \omega_1\tau + \phi_1). \tag{106}$$

In the case $\dot{q}_i = \dot{x}$ the proportionality between the left and right members for every τ is impossible, i.e. there is no solution for all $\tau \in [0,\infty]$ except for a set of values $\{\tau_k\}$ of measure zero. The main reason is that the right member of (106) describes an oscillating function with crossings by zero, mainly due to the monotonically increasing argument $\omega_1\tau$ with bounded signals $x(\tau)$, $y(\tau)$ and $\psi(\tau)$. For $\dot{x}(\tau)|\dot{x}(\tau)|$ to change oscillatory also the modes $y(\tau)$ and $\psi(\tau)$ will be varied in particular forms in τ. But these will result from the fundamental constrain represented by the dynamic equation (49). The same argumentation can be concluded for the other cases $\dot{q}_i \in \{\dot{y}, \dot{z}, \dot{\varphi}, \dot{\theta}, \dot{\psi}\}$.

On the other side, (101) concerns other differential equation of the same characteristic as (106). It is thus straightforward to conclude that this new equation has no solution for all $\tau \in [0,\infty]$ except for a set of values $\{\tau_k\}$ of measure zero.

For (102), the following differential equation

$$-\dot{q}_i(\tau)|\dot{q}_i(\tau)| = c_3 a_1^2, \tag{107}$$

is established and the solution for this is

$$q_i(\tau) = c_0\tau = \begin{cases} c_0 > 0, & c_0 = -\sqrt{c_3 a_1^2}, \\ c_0 < 0, & c_0 = \sqrt{c_3 a_1^2}, \end{cases} \tag{108}$$

with $c_3>0$. But this solution corresponds to an unbounded trajectory, which contradicts the stable solutions of the fundamental dynamic Eq. (49). So, we can infer that no state q_i can behave as $c_0 t$ and hence (102) cannot be satisfied for all $\tau\in[0,\infty]$ except for a set of measure zero. The same is inferred for (104) and (105).

It remains (103). This condition generates the constrain

$$\begin{aligned}&\cos(-k_1(x(\tau)-x_b)\cos(\beta-\psi(\tau))-k_1(y(\tau)-y_b)\sin(\beta-\psi(\tau))+\omega_1\tau+\phi_1)\\&\quad=c_4\sin(-k_1(x(\tau)-x_b)\cos(\beta-\psi(\tau))-k_1(y(\tau)-y_b)\sin(\beta-\psi(\tau))+\omega_1\tau\\&\qquad+\phi_1),\end{aligned}\tag{109}$$

which leads to

$$\begin{aligned}&\cos(\vartheta(x(\tau),y(\tau),\psi(\tau))+\omega_1\tau+\phi_1)\\&\quad=c_4\sin(\vartheta(x(\tau),y(\tau),\psi(\tau))+\omega_1\tau+\phi_1),\end{aligned}\tag{110}$$

with

$$\vartheta(x,y,\psi)=-k_1(x-x_b)\cos(\beta-\psi)-k_1(y-y_b)\sin(\beta-\psi),\tag{111}$$

a common function of the states in both arguments. Clearly, for every c_4 there exists a solution only for

$$\vartheta(x(\tau),y(\tau),\psi(\tau))+\omega_1\tau+\phi_1=\tan^{-1}\left(\frac{1}{c_4}\right),\tag{112}$$

which is satisfied by a set of countable τ_k's with measure zero in $[0,\infty]$.

So one can infer that properties (100)–(105) cannot be fulfilled, unless $c_j=0$ in $\tau\in[t, t+T_0]$, for every $t\in[0,\infty]$ and $T_0>0$. Finally on concludes that the regressor spans uniformly the space $\Re^4$ in $\tau\in[t,t+T_0]$ for $t\in[0,\infty]$ and $T_0>0$.

□

Theorem 2 (Persistency of Excitation—Case multichromatic waves). *If the floating structure is excited by a multichromatic wave elevation*

$$\begin{aligned}\xi(t,x,y)=\sum_{i=1}^{N}a_i\cos(&-k_i(x(t)-x_b)\cos(\beta-\psi(t))-k_i(y(t)-y_b)\sin(\beta-\psi(t))\\&+\omega_i t+\phi_i),\end{aligned}\tag{113}$$

then the regressor (40) *is PE.*

Proof. The PE condition of $\mathbf{\Phi}_{q_i}(\tau)$ on $\tau\in[t,t+T_0]$ is equivalent to

$$\text{span}\{\mathbf{\Phi}_{q_i}(\tau)\quad\text{on}\quad\tau\in[t,t+T_0]\}=\Re^{2(N+1)},\tag{114}$$

for every $T_0>0$ and $2(N+1)$ being the dimension of the parameter vector. Let the function

basis

$$B(t) = \{b_1(\tau), \ldots, b_{2N+2}\}, \tag{115}$$

be defined for generating vectors in $\Re^{2(N+1)}$ for specific τ.

The condition (114) is not satisfied if at least one of the following equations is fulfilled with $c_j = \text{constant} \neq 0$ in $\tau \in [t, t+T_0]$

$$b_1(\tau) = c_1 b_2(\tau), \tag{116}$$

$$b_1(\tau) = c_{2N+1} b_{2N+2}(\tau), \tag{117}$$

$$b_2(\tau) = c_{2N+2} b_3(\tau), \tag{118}$$

$$b_2(\tau) = c_{4N+1} b_{2N+2}(\tau), \tag{119}$$

$$b_{2N+1}(\tau) = c_{2N^2+3N+1} b_{2N+2}(\tau). \tag{120}$$

Many of these conditions are similar to those already analyzed in Theorem 1, where it was shown that those concerning trigonometric functions are not satisfied, unless $c_j = 0$. Therefore, these similar ones are also valid here. The rest of the conditions, however, involves two trigonometric functions of different frequencies and phases. They are, for instance, $b_2(\tau) = c_{2N+3} b_4(\tau)$, $b_2(\tau) = c_{2N+4} b_5(\tau)$, etc. In general, this class of equations can be put into

$$\sin(\vartheta(x(\tau), y(\tau), \psi(\tau)) + \omega_i \tau + \phi_i) = c_j \sin(\vartheta(x, (\tau) y(\tau), \psi(\tau)) + \omega_j \tau + \phi_j), \tag{121}$$

with ϑ defined in (111) and $\omega_i > \omega_j$. Invoking the boundedness of $x(\tau)$, $y(\tau)$ and $\psi(t)$, there are in general a countable number of real values τ_k in $[0, \infty]$ that are solution of (121). The set of τ_k's has measure zero.

Therefore, it can be concluded that the regressor $\mathbf{\Phi}_{q_i}$ spans the dimension of the parameter vector on $[t, t+T_0]$. As this will occur for every $T_0 > 0$ and $t \in [0, \infty]$, this span is uniform in $[0, \infty]$. Then $\mathbf{\Phi}_{q_i}$ is PE.

□

Now the proof of the convergence of the parameter trajectories $\boldsymbol{\theta}_{q_i}(t)$ is given. The demonstration is based on stability analysis via Lyapunov functions (see Ioannou and Sun, 1995). The analysis of both the asymptotic and the exponential convergence is placed under a common formalism. This in turn is related below to the fundamental estimators described before, namely the least squares-based and the gradient-based algorithms.

Theorem 3 (Asymptotic convergence). *If* $\mathbf{\Phi}_{q_i}(t)$ of (40) *is PE, then the pure least squares estimation of* (47) and (48) *gives asymptotically error-free estimates provided that the*

measures in the set

$$\mathcal{M}_i = \{\xi, q_i, \dot{q}_i, \ddot{q}_i, F_{q_i}\}, \tag{122}$$

are noise free, for $q_i \in \{x,y,z,\varphi,\theta,\psi\}$, with the exception of F_{q_i}, which constitutes the perturbed component q_i of the measure vector in the left member of (38).

Proof. Let a Lyapunov function be

$$V(t) := \int_0^t (\boldsymbol{\Phi}_{q_i}^T(\tau)\tilde{\boldsymbol{\theta}}_{q_i}(\tau))^2 \mathrm{d}\tau = \tag{123}$$

$$\frac{\tilde{\boldsymbol{\theta}}_{q_i}(t)P_{q_i}^{-1}(t)\tilde{\boldsymbol{\theta}}_{q_i}(t)}{2}, \tag{124}$$

with $\tilde{\boldsymbol{\theta}}_{q_i}(t) = -\boldsymbol{\theta}_{q_i} - \boldsymbol{\theta}_{q_i}(t)$ the error of the estimate and $\bar{\boldsymbol{\theta}}_{q_i}$ the true estimate. Then

$$V(t+T) = V(t) - \int_t^{t+T} (\boldsymbol{\Phi}_{q_i}^T(\tau)\tilde{\boldsymbol{\theta}}_{q_i}(\tau))^2 \, \mathrm{d}\tau, \tag{125}$$

for any t and $T>0$. Using $\boldsymbol{\Phi}_{q_i}^T(\tau)\tilde{\boldsymbol{\theta}}_{q_i}(\tau) = \boldsymbol{\Phi}_{q_i}^T(\tau)\tilde{\boldsymbol{\theta}}_{q_i}(t) + \boldsymbol{\Phi}_{q_i}^T(\tau)(\tilde{\boldsymbol{\theta}}_{q_i}(\tau) - \tilde{\boldsymbol{\theta}}_{q_i}(t))$ and the inequality $(x+y)^2 \geq (1/2)x^2 - y^2$, it follows

$$\int_t^{t+T} (\boldsymbol{\Phi}_{q_i}^T(\tau)\tilde{\boldsymbol{\theta}}_{q_i}(\tau))^2 \mathrm{d}\tau \geq \tag{126}$$

$$\frac{1}{2}\int_t^{t+T} (\boldsymbol{\Phi}_{q_i}^T(\tau)\tilde{\boldsymbol{\theta}}_{q_i}(t))^2 \, \mathrm{d}\tau - \tag{127}$$

$$\int_t^{t+T} (\boldsymbol{\Phi}_{q_i}^T(\tau)(\tilde{\boldsymbol{\theta}}_{q_i}(\tau) - \tilde{\boldsymbol{\theta}}_{q_i}(t)))^2 \, \mathrm{d}\tau. \tag{128}$$

Since $\boldsymbol{\Phi}_{q_i}$ is PE, one holds

$$\int_t^{t+T_0} \boldsymbol{\Phi}_{q_i}(\tau)\boldsymbol{\Phi}_{q_i}^T(\tau)\mathrm{d}\tau \geq \alpha_0 T_0 I \tag{129}$$

with $\alpha_0 > 0$ and some $T_0 > 0$, it follows from (124)

$$\int_t^{t+T_0} (\boldsymbol{\Phi}_{q_i}^T(\tau)\tilde{\boldsymbol{\theta}}_{q_i}(t))^2 \, \mathrm{d}\tau \geq \alpha_0 T_0 \tilde{\boldsymbol{\theta}}_{q_i}^T(t)\tilde{\boldsymbol{\theta}}_{q_i}(t). \tag{130}$$

On the other hand, the covariance matrix of the regressor $\boldsymbol{\Phi}_{q_i}$ is

$$\dot{P}_{q_i} = -P_{q_i}\boldsymbol{\Phi}_{q_i}\boldsymbol{\Phi}_{q_i}^T P_{q_i}, \qquad P_{q_i}(0) = P_{q_{i_0}}, \tag{131}$$

with $\dot{P}_{q_i} \leq 0$, i.e. $P_{q_i}(t) \leq P_{q_{i_0}}$. Moreover as $P_{q_i}(t)$ is nonincreasing and bounded from below, i.e. $P_{q_i}(t) = P_{q_i}^T(t) \geq 0, \quad \forall t \geq 0$, it is valid

$$\lim_{t\to\infty} P_{q_i}(t) = \bar{P}_{q_i}, \tag{132}$$

where $\bar{P}_{q_i} = \bar{P}_{q_i}^T \geq 0$ is a constant matrix. Because

$$P_{q_i}(t) = \left[\int_0^t \boldsymbol{\Phi}_{q_i}(\tau)\boldsymbol{\Phi}_{q_i}^T(\tau)\mathrm{d}\tau\right]^{-1}, \tag{133}$$

and $\boldsymbol{\Phi}_{q_i}$ uniformly spans a space of the parameter vector dimension on $[0, \infty]$, then $\bar{P}_{q_i} = 0$. Hence

$$\lambda_{\min}(t)I \leq P_{q_i}(t) \leq \lambda_{\max}(t)I, \tag{134}$$

with

$$\lim_{t\to\infty} \lambda_{\min}(t) = \lim_{t\to\infty} \lambda_{\max}(t) = 0, \tag{135}$$

and there also exist two bounds

$$\underline{\lambda}(t) \leq \lambda_{\min}(t) \leq \lambda_{\max}(t) \leq \bar{\lambda}(t), \tag{136}$$

with the properties

$$\underline{\lambda}(t) > \underline{\lambda}(t+\varepsilon), \tag{137}$$

$$\bar{\lambda}(t) < \bar{\lambda}(t+\varepsilon), \tag{138}$$

for $\varepsilon > 0$, i.e. $\underline{\lambda}(t)$ and $\bar{\lambda}(t)$ are monotonically increasing functions.

Using (124) and (134) in (130) one gets

$$\int_t^{t+T_0} (\boldsymbol{\Phi}_{q_i}^T(\tau)\tilde{\boldsymbol{\theta}}_{q_i}(t))^2 \, \mathrm{d}\tau, \tag{139}$$

$$\geq 2\alpha_0 T_0 \underline{\lambda}(t) V(t). \tag{140}$$

On the other side, it is valid from (47)

$$\tilde{\boldsymbol{\theta}}_{q_i}(\tau)-\tilde{\boldsymbol{\theta}}_{q_i}(t)= \tag{141}$$

$$\int_t^\tau \dot{\tilde{\boldsymbol{\theta}}}(\sigma)\mathrm{d}\sigma = \tag{142}$$

$$-\int_t^\tau P_{q_i}(\sigma)\boldsymbol{\Phi}_{q_i}(\sigma)\boldsymbol{\Phi}_{q_i}^T(\sigma)\tilde{\boldsymbol{\theta}}_{q_i}(\sigma)\mathrm{d}\sigma, \tag{143}$$

and it follows

$$\boldsymbol{\Phi}_{q_i}^T(\tau)(\tilde{\boldsymbol{\theta}}_{q_i}(\tau)-\tilde{\boldsymbol{\theta}}_{q_i}(t))=-\int_t^\tau \tilde{\boldsymbol{\theta}}_{q_i}^T(\sigma)\boldsymbol{\Phi}_{q_i}(\sigma)\boldsymbol{\Phi}_{q_i}^T(\tau)P_{q_i}(\sigma)\boldsymbol{\Phi}_{q_i}(\sigma)\mathrm{d}\sigma. \tag{144}$$

Using the Schwarz inequality on (128) with (144)

$$\int_t^{t+T_0} (\boldsymbol{\Phi}_{q_i}^T(\tau)(\tilde{\boldsymbol{\theta}}_{q_i}(\tau)-\tilde{\boldsymbol{\theta}}_{q_i}(t)))^2\,\mathrm{d}\tau \tag{145}$$

$$\leq \int_t^{t+T_0}\left(\int_t^\tau (\boldsymbol{\Phi}_{q_i}^T(\tau)P_{q_i}(\sigma)\boldsymbol{\Phi}_{q_i}(\sigma))^2\,\mathrm{d}\sigma\right)\left(\int_t^\tau (\boldsymbol{\Phi}_{q_i}^T(\sigma)\tilde{\boldsymbol{\theta}}_{q_i}(\sigma))^2\,\mathrm{d}\sigma\right)\mathrm{d}\tau, \tag{146}$$

$$\leq \beta^4\bar{\lambda}^2(t)\int_t^{t+T_0}(\tau-t)\int_t^\tau (\boldsymbol{\Phi}_{q_i}^T(\sigma)\tilde{\boldsymbol{\theta}}_{q_i}(\sigma))\mathrm{d}\sigma\mathrm{d}\tau, \tag{147}$$

with $\beta=\sup_{\tau\geq 0}|\boldsymbol{\Phi}_{q_i}(\tau)|$. Changing the sequence of integration in (147), it is valid

$$\int_t^{t+T_0} (\boldsymbol{\Phi}_{q_i}^T(\tau)(\tilde{\boldsymbol{\theta}}_{q_i}(\tau)-\tilde{\boldsymbol{\theta}}_{q_i}(t)))^2\,\mathrm{d}\tau, \tag{148}$$

$$\leq \beta^4\bar{\lambda}^2(t)\int_t^{t+T_0}(\boldsymbol{\Phi}_{q_i}^T(\sigma)\tilde{\boldsymbol{\theta}}_{q_i}(\sigma))^2\int_\sigma^{t+T_0}(\tau-t)\mathrm{d}\tau\mathrm{d}\sigma, \tag{149}$$

$$\leq \beta^4 \bar{\lambda}^2(t) \int_t^{t+T_0} (\boldsymbol{\Phi}_{q_i}^T(\sigma)\tilde{\boldsymbol{\theta}}_{q_i}(\sigma))^2 \left[\frac{T_0^2-(\sigma-t)^2}{2}\right] \mathrm{d}\sigma, \tag{150}$$

$$\leq \frac{\beta^4 \bar{\lambda}^2(t) T_0^2}{2} \int_T^{t+T_0} (\boldsymbol{\Phi}_{q_i}^T(\sigma)\tilde{\boldsymbol{\theta}}_{q_i}(\sigma))^2 \mathrm{d}\sigma. \tag{151}$$

Using (140) and (151) as new bounds for (127) and (128) in (126) and making $T=T_0$, one achieves

$$\int_t^{t+T_0} (\boldsymbol{\Phi}_{q_i}^T(\tau)\tilde{\boldsymbol{\theta}}_{q_i}(\tau))^2 \, \mathrm{d}\tau, \tag{152}$$

$$\geq \alpha_0 T_0 \underline{\lambda}(t) V(t) - \frac{\beta^4 \bar{\lambda}^2(t) T_0^2}{2} \int_T^{t+T_0} (\boldsymbol{\Phi}_{q_i}^T(\sigma)\tilde{\boldsymbol{\theta}}_{q_i}(\sigma))^2 \, \mathrm{d}\sigma, \tag{153}$$

which leads to

$$\int_t^{t+T_0} (\boldsymbol{\Phi}_{q_i}^T(\tau)\tilde{\boldsymbol{\theta}}_{q_i}(\tau))^2 \, \mathrm{d}\tau, \tag{154}$$

$$\frac{\geq 2\alpha_0 T_0 \underline{\lambda}(t)}{2 + \beta^4 T_0^2 \bar{\lambda}^2(t) V(t).} \tag{155}$$

Using this inequation in (125) for $T=T_0$ and denoting $\gamma_1(t) = (2\alpha_0 T_0 \underline{\lambda}(t))/(2 + \beta^4 T_0^2 \bar{\lambda}^2(t))$ one attains finally

$$V(t+T_0) \leq (1-\gamma_1(t))V(t) = \gamma(t)V(t). \tag{156}$$

Because $\gamma_1(t) \geq 0$ and $V(t+T_0) \geq 0$, then we have $0 < \gamma(t) < 1$.

Since (156) holds for all $t \geq 0$, we can take samples of $V(t)$ equally spaced at time points equal to nT_0, $n=0,1,\ldots$, and use (156) successively to obtain

$$V(t) \leq V(nT_0) \leq \gamma(0)\gamma(1)\cdots\gamma((n-1)T_0)V(0), \tag{157}$$

for all $t \geq nT_0$, and $0 < \gamma(0), \gamma(T_0), \ldots, \gamma((n-1)T_0) < 1$ with $\gamma(t) \to 1$ for $t \to \infty$. Certainly, as $n \to \infty$, $\prod_{i=0}^{n-1} \gamma(iT_0) \to 0$, and the convergence is reached asymptotically, i.e. $V(t) \to 0$ for $t \to \infty$ asymptotically fast. This implies in turn that $\tilde{\boldsymbol{\theta}}_{q_i}(t) \to 0$ for $t \to \infty$ asymptotically fast. □

Remark 1 (Exponential Convergence). As $\underline{\lambda}(t)$ and $\bar{\lambda}(t)$ are not guaranteed to be constant or time-variable with the same order of magnitude, then one can not ensure an exponential decay of $V(t)$ in time as in the case of a gradient-based algorithm, where $P_{q_i}(t)$ is replaced by a fixed positive definite matrix Γ in the adaptation law (46). As $\gamma(t)$ will tend to 1 asymptotically fast for t tending to infinity, a rapid approximation of the parameter trajectory is expected in the initial phase, while the convergence will go decelerating in time. On the contrary, for a gradient-based algorithm the descent of the error trajectory $\tilde{\boldsymbol{\theta}}_{q_i}(t)$ is uniform in time and takes place exponentially.

This can be drawn out directly from the last result in former theorem. If we replace $P_{q_i}(t)$ in the adaptation law by a constant, positive definite matrix Γ with constant eigenvalues $\lambda_{\max}$ and $\lambda_{\min}$, then $\gamma = 1 - ((2\alpha_0 T_0 \lambda_{\min})/(2 + \beta^4 T_0^2 \lambda_{\max}^2)) = \text{constant}$ and it is valid

$$V(t) \leq V(nT_0) \leq \gamma^n V(0), \quad \text{for} \quad \forall\, t \geq nT_0, \quad n = 0, 1, \ldots, \tag{158}$$

for all $t \geq nT_0$, $0 < \gamma^n < 1$, and the convergence occurs exponentially fast.

7. Case study: identification of a semisubmersible

In order to test the proposed estimation algorithms in Section 3, the model of a moored semisubmersible called Thialf (DB102) is taken as case study (see Fig. 13). The main geometric measures and operating parameters of the dynamic system are given in the table 2.

This kind of system has a complex hydrodynamics represented by the induced radiation, diffraction and incident forces. It disposes of six thrusters for pitch control during operation of the twin cranes. The structure is maintained at a fixed position by means of a system of mooring lines with symmetric balance of the initial tensions. For the

Fig. 13. Twin crane semisubmersible Thialf.

Table 2
Basic information of the semisubmersible model Thialf

Length (m)	Breadth (m)	Weight (ton)	Max. load (ton)	Min. draught (m)	Max. draught (m)
201.6	88.4	136,709	14,200	11.8	31.6

simulation of the whole dynamics, a geometric model was constructed in the program Advanced Quantitative Wave Analysis® (AQWA, 2002), see Fig. 2. The CAD program enables the calculation of the hydrodynamic forces by means of finite elements and the simulation of the behavior under external perturbations like regular waves. In all simulations it is assumed that the pitch control remains inactive and the structure stands at a static equilibrium before the wave action comes into effect on the system behavior. Moreover, a perfect symmetry in geometry and mass distribution about the plane x–z is assumed.

The simulations are divided into case (a) monochromatic excitation and case (b) multichromatic excitation. In the first case, the system is subject to a planar motion involving three modes of motion. In the second case, the system is free to move in six degrees of freedoms. The simulation provides all the measures, i.e. the signals on the first membership of (38) and the elevation of the free surface at the point O on the water line, so as the regression (39) for the parameter estimation can be built up with $\mathbf{s}_2(t) \equiv 0$. The estimation algorithm used in the simulation is based on quadratic norm and described in (47) and (48).

7.1. Parameter identification under monochromatic waves

Under symmetric distribution of mass and volume about the x–z plane, an incident angle for the monochromatic wave equal to zero will produced a planar motion of the system in the modes surge, heave and pitch. This kind of wave constitutes the most unfavorable case for the estimation from the viewpoint of the richness of the excitation.

In Table 3 the parameters of the monochromatic wave are given.

The steepness of the selected wave, i.e. $2a/\lambda$, is small enough ($2a/\lambda = 0.0186 < 1/50$) so as to consider the Potential Theory of Airy for the hydrodynamics valid. According to (41), the parameters to be identified are

$$\boldsymbol{\theta}_x = [\, C_{D_x} A_x \quad H_{1x} \quad H_{2x} \quad G_x \,]^{\mathrm{T}}, \tag{159}$$

$$\theta_z = [\, C_{D_z} A_z \quad H_{1z} \quad H_{2z} \quad G_z \,]^{\mathrm{T}}, \tag{160}$$

Table 3
Wave parameters

Frequency ω_0 (rad/s)	Period T (s)	Amplitude a (m)	Number k (rad/m)	Phase ϕ (rad)	Angle β (rad)	Length λ (m)	Depth d (m)
0.445	14.1354	2.8190	2.0237×10^{-2}	1.5736	0	302.34	100

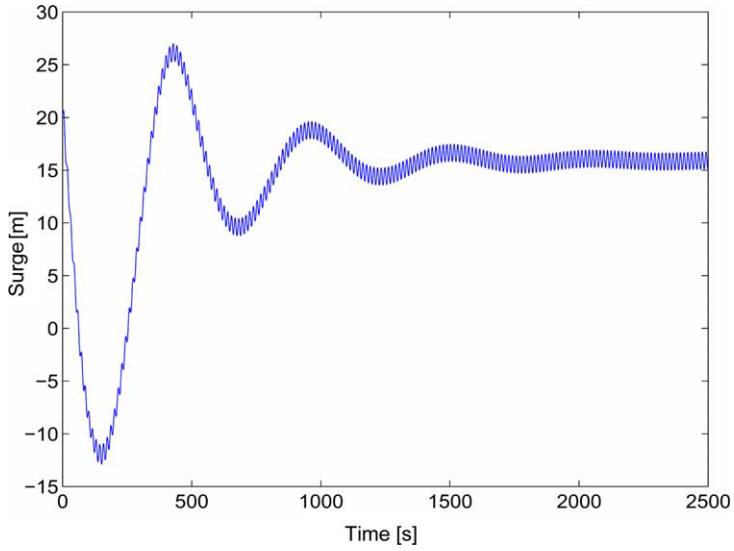

Fig. 14. Induced surge motion under monochromatic excitation.

$$\boldsymbol{\theta}_\theta = [\, C_{D_\theta} A_\theta \quad H_{1_\theta} \quad H_{2_\theta} \quad G_\theta \,]^{\mathrm{T}}. \tag{161}$$

Figs. 14–16 depict the evolution of the modes *surge*, *heave* and pitch of the semisubmersible, beginning from the static equilibrium up to practically the steady state. It is appreciated a transitory of great intensity and duration with a weak damping,

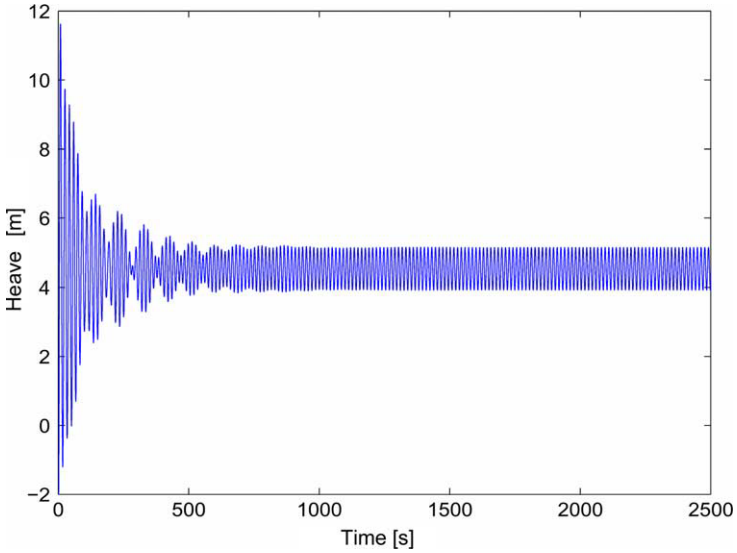

Fig. 15. Induced heave motion under monochromatic excitation.

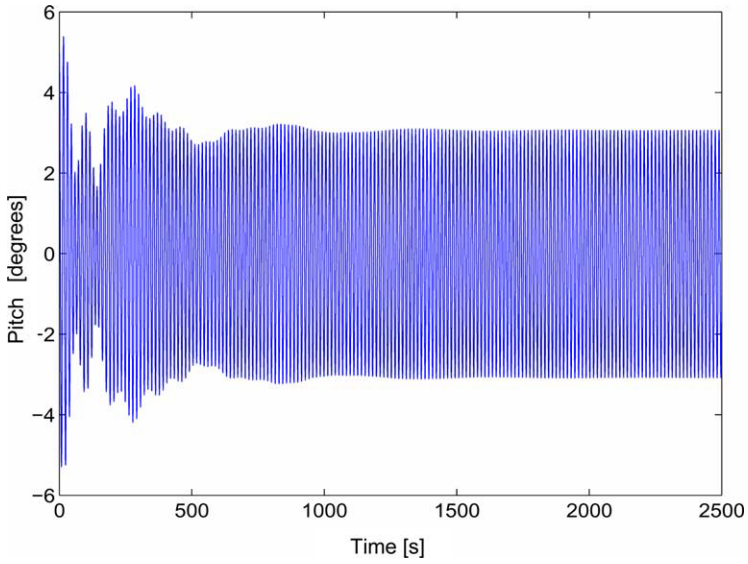

Fig. 16. Induced pitch motion under monochromatic excitation.

particularly in the *surge* mode. The long persistence of the transitions is mainly due to the large inertia and the weak potential-radiation and viscous damping under slow motions. The transient duration is approximately 170 times longer that the period of the wave in the surge mode, but about the half shorter in the heave and pitch modes.

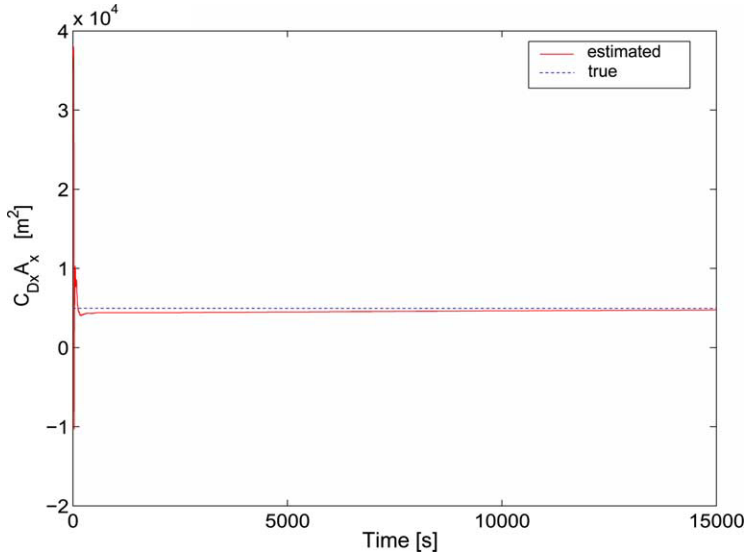

Fig. 17. Evolution of the estimate $C_{D_x}A_x$.

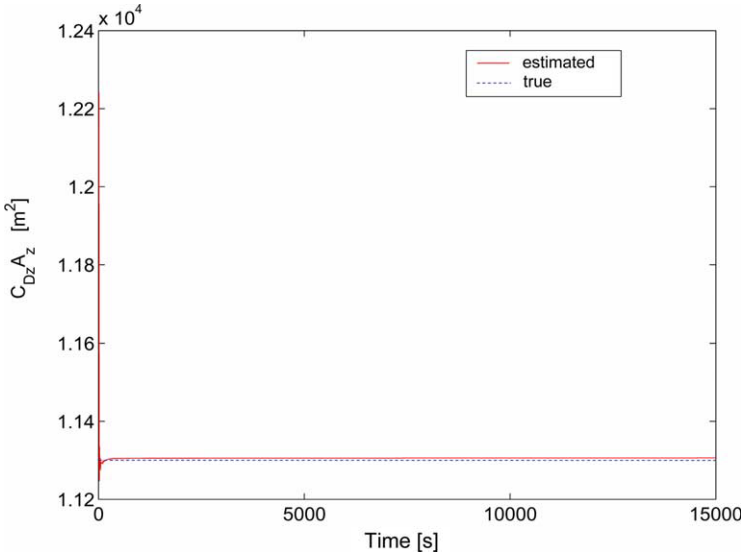

Fig. 18. Evolution of the estimate $C_{D_z}A_z$.

Figs. 17–19 reproduce the evolution of the estimates which contain the drag coefficients in the different modes. The true values of the C_{D_i}'s can indirectly be obtained if the effective areas A_x, A_z and A_θ are calculated beforehand. The convergence is fast in the first phase and then the evolution tends slowly to the true values with exception of the estimate $C_{D_\theta}A_\theta$, which shows a small bias at end of the identification period.

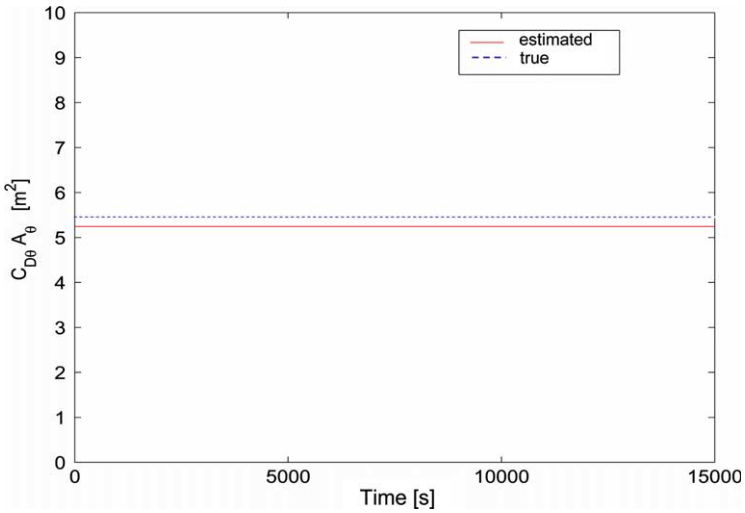

Fig. 19. Evolution of the estimate $C_{D_\theta}A_\theta$.

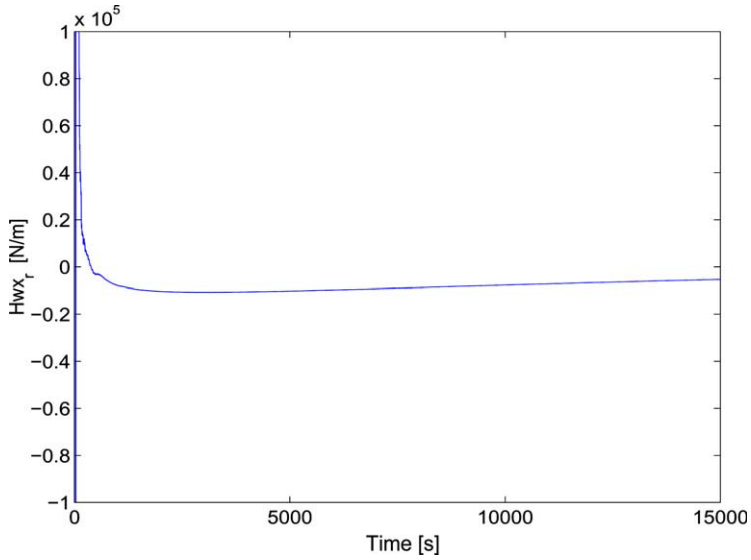

Fig. 20. Evolution of the estimate H_{1x}.

In Figs. 20–23, the behavior of the estimates for the incident force transfer function in the x–y plane are exposed. One sees the convergence takes place asymptotically.

The estimation of the constant parameters of the second-order drift force, are given in Figs. 24 and 25. A slow convergence is however observed in the estimate G_z.

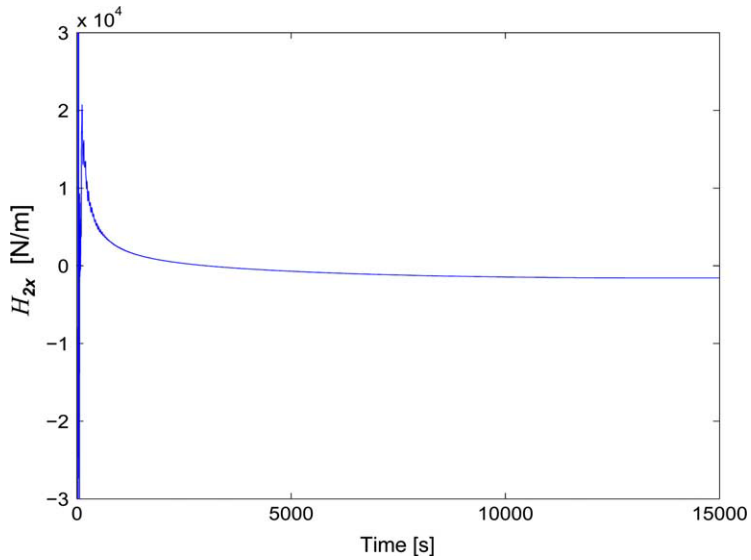

Fig. 21. Evolution of the estimate H_{2x}.

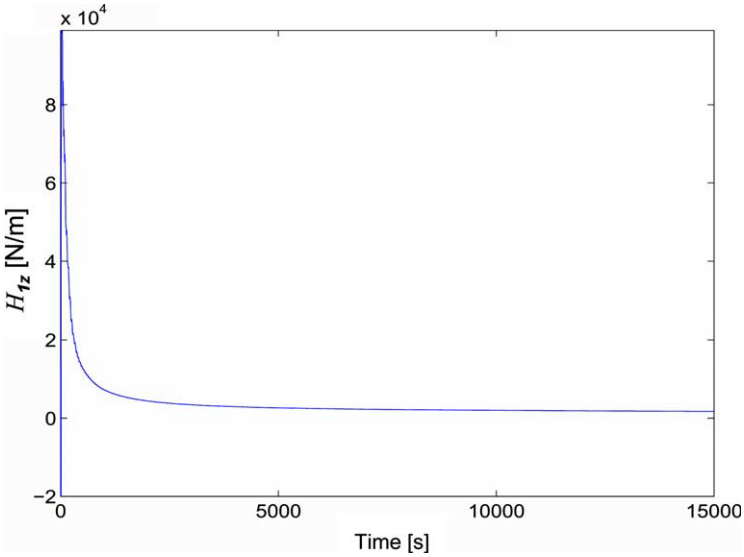

Fig. 22. Evolution of the estimate H_{1z}.

In general, the transient behavior has enabled a fast approximation of the estimates to the true values, yet for some parameters the asymptotic convergence takes place slow in steady state. The reason is that the level of excitation drops in time as it is verified from the evolution of the eigenvalues of the covariance matrix of the least-squares estimator for the

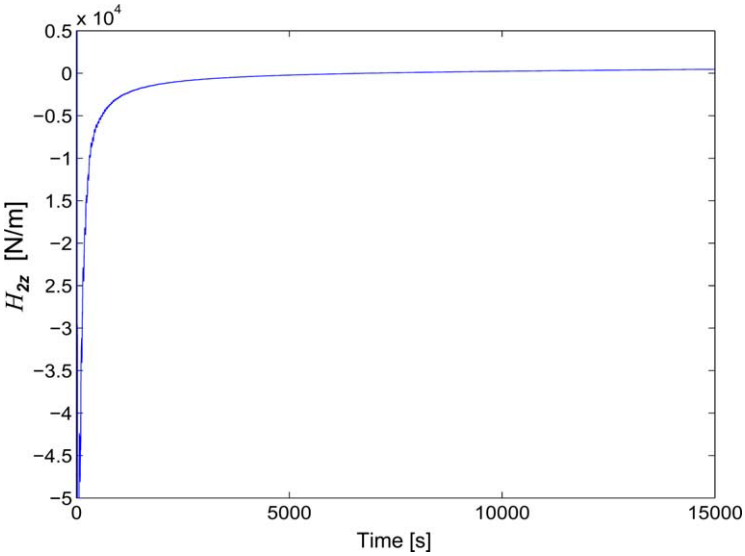

Fig. 23. Evolution of the estimate H_{2z}.

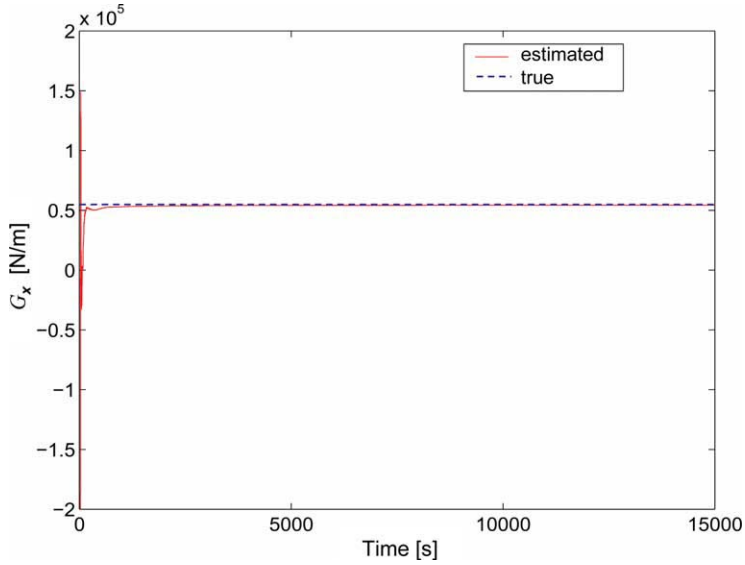

Fig. 24. Evolution of the estimate G_x.

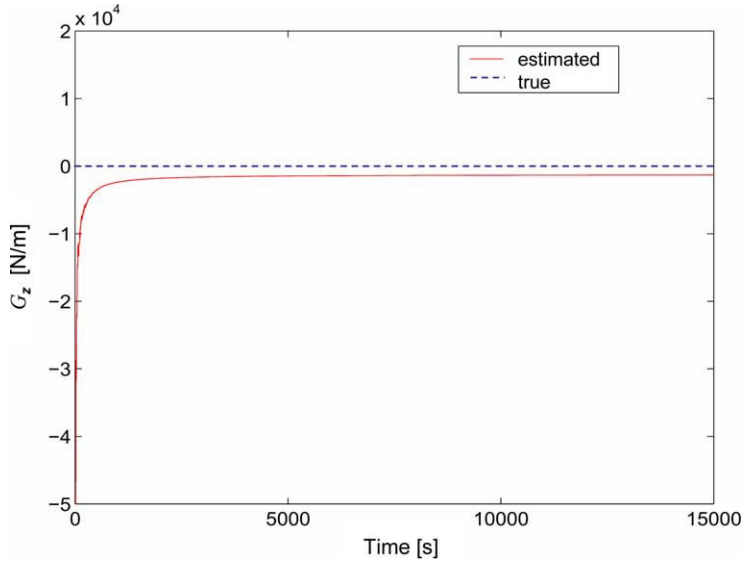

Fig. 25. Evolution of the estimate G_z.

mode q_i

$$P_{q_i}^{-1}(t) = \left[\int_0^t \mathbf{\Phi}_{q_i}(\tau)\mathbf{\Phi}_{q_i}^T(\tau)\mathrm{d}\tau\right]^{-1}, \tag{162}$$

and from its relation with the property of persistence of excitation PE (cf. (91))

$$\int_{t-T_0}^{v} \mathbf{\Phi}_{q_i}(\tau)\mathbf{\Phi}_{q_i}^T(\tau)\mathrm{d}\tau = P_{q_i}^{-1}(t) - P_{q_i}^{-1}(t-T_0). \tag{163}$$

In Fig. 26, the behavior in time of the eigenvalues of the covariance matrix for the parameter vector θ_x are shown as part of the validation for $P_x(t)>0$.

All eigenvalues remain positive during the estimation. From them, the second and the forth constitute the minimal and maximal values (referred to as $\underline{\lambda}$ and $\bar{\lambda}$), respectively. From (162) and (163) and the evolutions of $\underline{\lambda}$ and $\bar{\lambda}$ it is proved that there always exists an instant t_1 so that $t>t_1$ for which it is valid

$$[t\underline{\lambda}(t)-(t-T_0)\underline{\lambda}(t-T_0)]I$$

$$\leq \int_{t-T_0}^{t} \mathbf{\Phi}_{q_i}(\tau)\mathbf{\Phi}_{q_i}^T(\tau)\mathrm{d}\tau \leq [t\bar{\lambda}(t)-(t-T_0)\bar{\lambda}(t-T_0)]I, \tag{164}$$

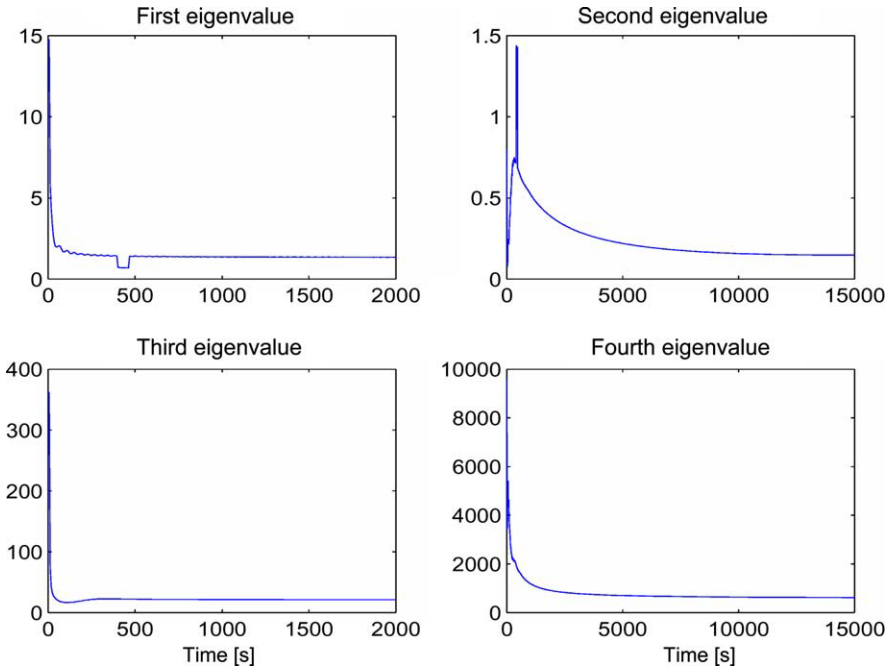

Fig. 26. Evolution of the eigenvalues of $(1/t)P^{-1}(t)$.

and there exist $\alpha_1,\alpha_0>0$ such that

$$\alpha_1 \geq [t\bar{\lambda}(t)-(t-T_0)\bar{\lambda}(t-T_0)] > [t\underline{\lambda}(t)-(t-T_0)\underline{\lambda}(t-T_0)] \geq \alpha_0, \tag{165}$$

for every $T_0>0$. The same is verified for the eigenvalues of the minors of first, second and third order. Then, for $t\to\infty$ it is expected an asymptotic convergence of the estimates from $\theta_x(0)$.

7.2. Parameter identification under multichromatic waves

In this case a multichromatic wave with an incident angle of 45° is applied to excite the floating structure in 6 degrees of freedom. The wave parameters are summarized in Table 4.

For this case there are 72 parameters involved to be estimated. They are described in the parameter vectors

$$\boldsymbol{\theta}_x\left(\omega_0,\beta=\frac{\pi}{4}\right) = \left[\, C_{D_x}A_x \quad H_{1x_1}\ldots H_{1x_{10}} \quad H_{2x_1}\ldots H_{2x_{10}} \quad G_x \,\right]^{\mathrm{T}}, \tag{166}$$

$$\boldsymbol{\theta}_y\left(\omega_0,\beta=\frac{\pi}{4}\right) = \left[\, C_{D_y}A_y \quad H_{1y_1}\ldots H_{1y_{10}} \quad H_{2y_1}\ldots H_{2y_{10}} \quad G_y \,\right]^{\mathrm{T}}, \tag{167}$$

$$\boldsymbol{\theta}_z\left(\omega_0,\beta=\frac{\pi}{4}\right) = \left[\, C_{D_z}A_z \quad H_{1z_1}\ldots H_{1z_{10}} \quad H_{2z_1}\ldots H_{2z_{10}} \quad G_z \,\right]^{\mathrm{T}}, \tag{168}$$

$$\boldsymbol{\theta}_\varphi\left(\omega_0,\beta=\frac{\pi}{4}\right) = \left[\, C_{D_\varphi}A_\varphi \quad H_{1\varphi_1}\ldots H_{1\varphi_{10}} \quad H_{2\varphi_1}\ldots H_{2\varphi_{10}} \quad G_\varphi \,\right]^{\mathrm{T}}, \tag{169}$$

$$\boldsymbol{\theta}_\theta\left(\omega_0,\beta=\frac{\pi}{4}\right) = \left[\, C_{D_\theta}A_\theta \quad H_{1\theta_1}\ldots H_{1\theta_{10}} \quad H_{2\theta_1}\ldots H_{2\theta_{10}} \quad G_\theta \,\right]^{\mathrm{T}}, \tag{170}$$

$$\boldsymbol{\theta}_\psi\left(\omega_0,\beta=\frac{\pi}{4}\right) = \left[\, C_{D_\psi}A_\psi \quad H_{1\psi_1}\ldots H_{1\psi_{10}} \quad H_{2\psi_1}\ldots H_{2\psi_{10}} \quad G_\psi \,\right]^{\mathrm{T}}. \tag{171}$$

Table 4
Harmonic components of a multichromatic wave for simulation

Comp. j	Freq. ω (rad/s)	Period T (s)	Amplit. a (m)	Number k (rad/m)	Phase ϕ (rad)	Angle β (rad)	Length λ (m)	Depth d (m)
1	0.272	23.099	0.312	8.743×10^{-3}	1.572	π/4	632.292	100
2	0.309	20.333	0.433	1.058×10^{-2}	48.923	π/4	533.637	100
3	0.334	18.811	0.325	1204×10^{-2}	273.587	π/4	478.082	100
4	0.358	17.550	0.404	1.357×10^{-2}	166.684	π/4	431.353	100
5	0.384	16.362	0.304	1.534×10^{-2}	193.366	π/4	386.756	100
6	0.413	15.213	0.290	1.757×10^{-2}	80.395	π/4	343.233	100
7	0.448	14.025	0.424	2.059×10^{-2}	18.506	π/4	298.165	100
8	0.496	12.667	0.334	2.518×10^{-2}	245.961	π/4	247.416	100
9	0.575	10.927	0.286	3.373×10^{-2}	246.116	π/4	185.986	100
10	0.852	7.376	0.296	7.415×10^{-2}	338.059	π/4	84.943	100

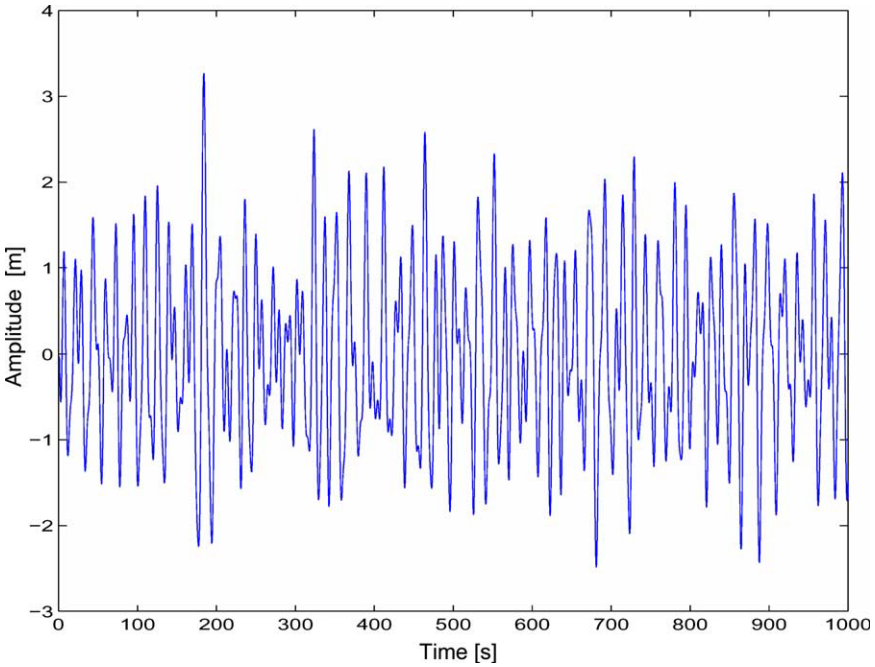

Fig. 27. Multichromatic wave excitation of 10 components.

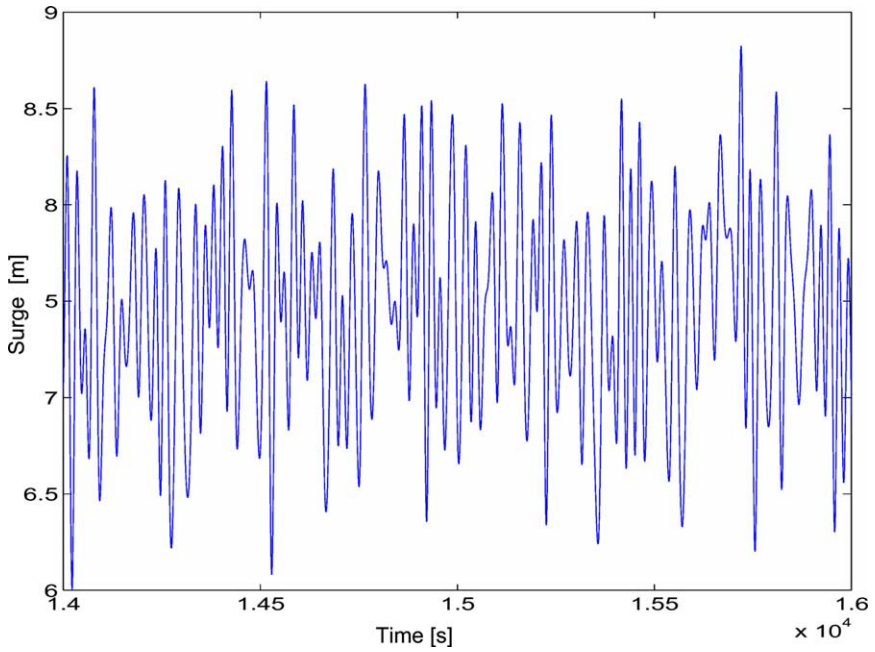

Fig. 28. Evolution of the surge mode.

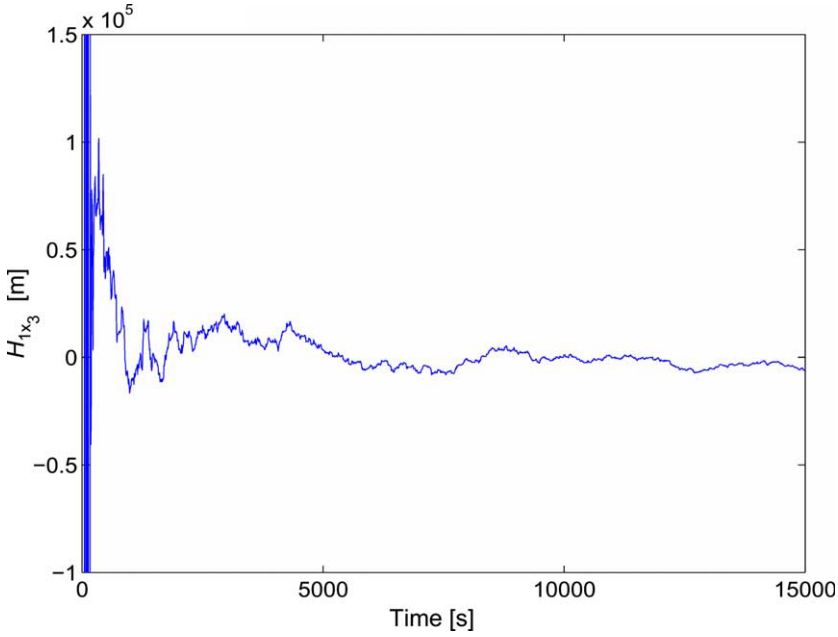

Fig. 29. Evolution of the estimate H_{1x_3}.

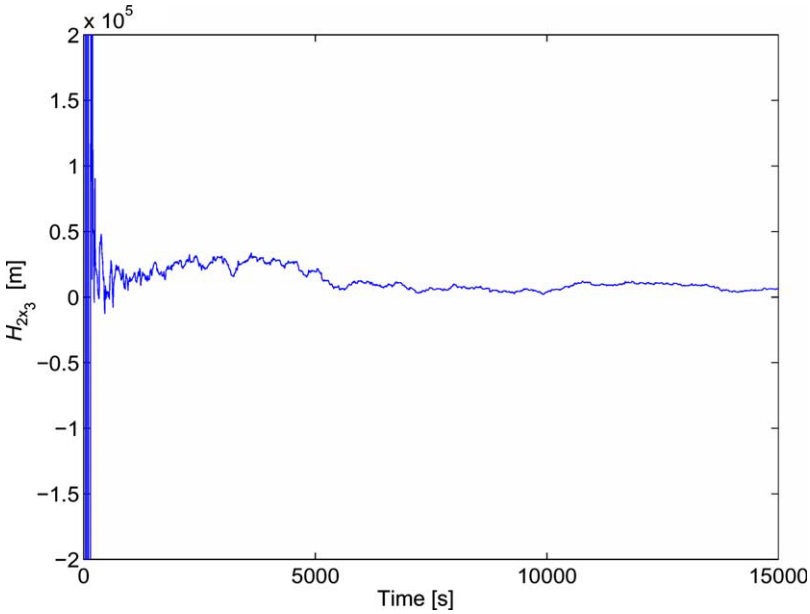

Fig. 30. Evolution of the estimate H_{2x_3}.

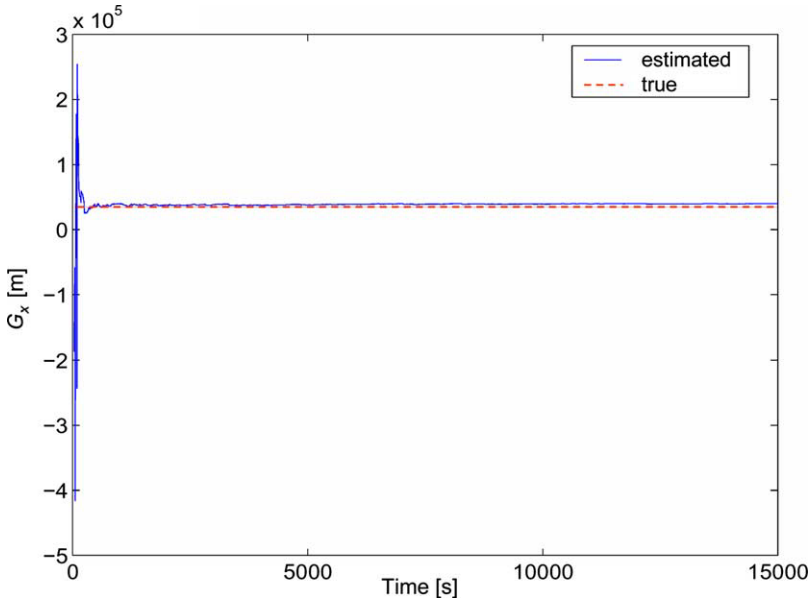

Fig. 31. Evolution of the estimate G_x.

The surface elevation is given in Fig. 27. From this excitation it results the surge displacement x as shown in Fig. 28.

In the next figures a part of the estimations are depicted. All evolutions corresponding to the first-order components of the exciting force parameters are characterized by a fast convergence after starting the estimation followed by a jittery behavior of the estimates about a fixed value. The variance of the estimates however fades away in time. These features can be observed in Figs. 29 and 30 for the parameters corresponding to the third harmonic of the wave in the sway mode.

The evolution of the estimations corresponding to the second-order components of the exciting force parameters is, in opposite to those of the first-order components, smooth and faster. As example of these features the estimate for the surge mode is reproduced in Fig. 31.

8. Conclusions

In this work an approach to identify hydrodynamic models for incident, diffraction and viscous forces acting on a moored floating structure is presented. It is based on measures of the mechanical state and of the mooring forces. This contribution, together with the identification of models for the mooring lines attached to the structure (Jordán and Beltrán-Aguedo, 2004a) and the estimation of potential-radiation models (Jordán and Beltrán-Aguedo, 2004b) complete the parameter estimation of the whole dynamic system.

An important aspect in the approach has consisted in the analysis of the unknown initial condition of the hydrodynamic state for the potential-radiation force. It has been proved that its influence on the parameter convergence is vanishing and has no long-term effect. The number of parameters of the hydrodynamics involved in the estimation is relatively large. Due to the nonlinear nature of the model structure, it is possible to satisfy a complete span of the regressor (PE property) even in the case of poor excitation conditions. This work has provided theoretical results that show that asymptotic convergence of the estimates takes place under arbitrary conditions of the wave excitation. The proof was given first for the case of monochromatic waves, which can be considered as the worst case from the viewpoint of the richness of information. This result was also generalized for the case of multichromatic waves. A case study consisting in the identification of a moored semisubmersible shows the application of the approach by means of numerical simulations.

Acknowledgements

The author thanks Prof. Dr.-Ing. Edwin Kreuzer and Dr-Ing. Volker Schlegel at the Technical University of Hamburg-Harburg for the theoretical support in Hydrodynamics, and Dr Reinel Beltrán-Aguedo for the realization of the simulations. Also it is thanked the National Council for Science and Technology, Argentine and the Universidad Nacional del Sur for the financial support of this investigation.

References

AQWA, 2002. AQWA Reference Manual, Version 5.3A. Century Dynamics Ltd.

Borgman, L.E., Niedzwecki, J., Scheffner, N.W., Kern, J.W., Petrakos, M., 2003. Statistical analysis of ocean waves and other environmental data. Advanced Series on Ocean Engineering. World Scientific, Singapore.

Bracewell, R.N., 1978. The Fourier Transform and its Applications. McGraw-Hill, Kogakusha.

Chakrabarti, S.K., 1994. Offshore Structure Modeling. World Scientific, Singapore.

Clauss, G., Sükan, M., Schellin, T.E., 1982. Drift forces on compact offshore structures in regular and irregular waves. Journal of Applied Ocean Research 4 (4), 208–218.

Cummins, W.E., 1962. The impulse response function and ship motions. Schiffstechnik 9 (1), 101–109.

Faltisen, O.M., 1990. Sea Loads on Ships and Offshore Structures. Cambridge University Press, Cambridge.

Fossen, T.I., 1994. Guidance and Control of Ocean Vehicles. Wiley, London.

Grosenbaugh, M.A., 1996. On the dynamics of oceanographic surface moorings. Ocean Engineering 23 (1), 7–25.

Ioannou, P., Sun, J., 1995. Robust Adaptive Control. PTR Prentice-Hall, Upper Saddle River.

Jiang, T., 1991. Untersuchung nichtlinearer Schiffsdynamik mit Auftreten von Instabilität und Chaos an Beispielen aus der Offshoretechnik. Technical Report Nr. 512. PhD Thesis, Institut für Schiffbau der Universität Hamburg, Germany.

Jordán, M.A., 2002. Input design: a method for achieving persistency of excitation in nonlinear parametrized systems. 15th IFAC World Congress, July 21–26, Barcelona, Spain.

Jordán, M.A., Beltrán-Aguedo, R., 2003. Optimal identification of hydrodynamics for marine structures and vehicles—two general approaches in time-domain. Proceedings of RPIC'03, San Nicolas, Argentina.

Jordán, M.A., Beltrán-Aguedo, R., 2004a. Nonlinear identification of mooring lines in dynamic operation of floating structures. Ocean Engineering 31, 455–482.

Jordán, M.A., Beltrán-Aguedo, R., 2004b. Optimal identification of potential-radiation hydrodynamics for moored floating structures a new general ppproach in state space. Ocean Engineering 31, 1859–1914.

Kreisselmeier, G., Rietze-Augst, G., 1990. Richness and excitation on an interval—with applications to continuous-time adaptive control. IEEE Transactions on Automatic Control 35 (2), 165–171.

Kreuzer, E., Ellermann, K., Markiewicz, M., 2002. Nonlinear dynamics of floating cranes. Nonlinear Dynamics 27, 107–183.

Ljung, L., 1987. System Identification—Theory for the User. PTR Prentice-Hall, Englewood Cliffs, NJ.

Narendra, K.S., Annaswamy, A.M., 1987. Persistency of excitation in adaptive sysytems. International Journal of Control 45 (1), 127–160.

Olgivie, T.F., 1964. Recent progress toward the understanding and prediction of ship motions. Symposium on Naval Hydrodynamic. ONR, Washington, DC, pp. 3–128.

Schelin, T.E., Jiang, T., Östergaard, C., 1993. Response analysis and operating limits of crane ships. Journal of Ship Research 37, 225–238.

Sorensen, R.M., 1993. Basic Wave Mechanics: For Coastal and Ocean Engineering, Wiley–Interscience.

Tasai, F., Kawatate, K., Ohkusu, M., Koterayama, W., 1980. A single point mooring spar buoy for measuring ocean waves. Ocean Engineering 7 (1), 173–192.